Article

Noncoding translation mitigation

https://doi.org/10.1038/s41586-023-05946-4

Received: 27 July 2022

Accepted: 13 March 2023

Published online: 12 April 2023

Check for updates

Jordan S. Kesner[1,2,5], Ziheng Chen[1,2,4,5], Peiguo Shi[1,2], Alexis O. Aparicio[1,2], Michael R. Murphy[1,2], Yang Guo[1,2], Aditi Trehan[1,2], Jessica E. Lipponen[3], Yocelyn Recinos[2], Natura Myeku[3] & Xuebing Wu[1,2]✉

Translation is pervasive outside of canonical coding regions, occurring in long noncoding RNAs, canonical untranslated regions and introns[1–4], especially in ageing[4–6], neurodegeneration[5,7] and cancer[8–10]. Notably, the majority of tumour-specific antigens are results of noncoding translation[11–13]. Although the resulting polypeptides are often nonfunctional, translation of noncoding regions is nonetheless necessary for the birth of new coding sequences[14,15]. The mechanisms underlying the surveillance of translation in diverse noncoding regions and how escaped polypeptides evolve new functions remain unclear[10,16–19]. Functional polypeptides derived from annotated noncoding sequences often localize to membranes[20,21]. Here we integrate massively parallel analyses of more than 10,000 human genomic sequences and millions of random sequences with genome-wide CRISPR screens, accompanied by in-depth genetic and biochemical characterizations. Our results show that the intrinsic nucleotide bias in the noncoding genome and in the genetic code frequently results in polypeptides with a hydrophobic C-terminal tail, which is captured by the ribosome-associated BAG6 membrane protein triage complex for either proteasomal degradation or membrane targeting. By contrast, canonical proteins have evolved to deplete C-terminal hydrophobic residues. Our results reveal a fail-safe mechanism for the surveillance of unwanted translation from diverse noncoding regions and suggest a possible biochemical route for the preferential membrane localization of newly evolved proteins.

How cells faithfully decode the genome to synthesize a functional proteome is a fundamental question in modern biology. Although the fidelity of transcription and translation are high, the substrate specificities that dictate which DNA regions are transcribed and which RNA molecules are translated are rather low, resulting in pervasive transcription of the genome[22] and widespread translation in noncoding regions of the transcriptome, such as untranslated regions (UTRs), introns and long noncoding RNAs[1–4] (lncRNAs). Furthermore, these aberrant translational activities are increased in ageing[4–6], neurodegeneration[5,7] and cancer[8–10], owing to the impairment of mRNA splicing and polyadenylation[7,23–25], mRNA quality control[26–28] and translation termination[10,29]. Consequently, peptides derived from noncoding regions account for the majority of tumour-specific antigens[11–13] and tend to be associated with unfavourable prognoses for patients[30].

Despite the prevalence of translation in noncoding sequences and its probably important contributions to disease pathogenesis, the surveillance mechanisms preventing the accumulation of potentially toxic aberrant translation products remain poorly understood. So far, relevant studies have focused primarily on 3′ UTR translation in a small set of genes and have reached conflicting conclusions regarding the role of ribosome stalling[16,17], proteasomal degradation[10,18] and lysosomal aggregation[19]. Alongside these results, the lack of studies involving lncRNAs, introns and 5′ UTRs underscores the need for more systematic investigations aimed at uncovering potential unifying principles for the surveillance of translation in diverse types of noncoding sequences.

Although most aberrant translation products are likely to be nonfunctional, on the evolutionary timescale, translation in noncoding sequences is necessary to expose the noncoding genome to natural selection and to facilitate the origination of new protein-coding genes. Studies have identified many functional peptides translated from previously annotated lncRNAs in mammalian cells[20,21]. Among 64 functional peptides whose cellular localization has been determined experimentally, about three-quarters (47) localize to the plasma membrane or organelle membranes (Supplementary Table 1). Similarly, studies in yeast show that proto-genes (translated non-genic sequences) tend to encode putative transmembrane regions[14,15]. However, the biochemical mechanism that allows polypeptides derived from noncoding sequences to escape cellular surveillance and preferentially localize to membranes remains unknown.

Here, by combining unbiased high-throughput screens with in-depth dissection of individual cases, we present a unified model for the mitigation of translation in diverse noncoding sequences, which also provides insights into the preferential membrane targeting of newly evolved proteins.

Non-canonical proteins are unstable

A common outcome of translation in various noncoding contexts is that the resulting polypeptide has a C-terminal tail derived from annotated noncoding sequences (Fig. 1a, light blue). We constructed reporters

[1]Cardiometabolic Genomics Program, Division of Cardiology, Department of Medicine, Columbia University Irving Medical Center, New York, NY, USA. [2]Department of Systems Biology, Columbia University Irving Medical Center, New York, NY, USA. [3]Taub Institute for Research on Alzheimer's Disease and the Aging Brain, Department of Pathology and Cell Biology, Columbia University Irving Medical Center, New York, NY, USA. [4]Present address: Department of Biological Sciences, Carnegie Mellon University, Pittsburgh, PA, USA. [5]These authors contributed equally: Jordan S. Kesner, Ziheng Chen. ✉e-mail: xw2629@cumc.columbia.edu

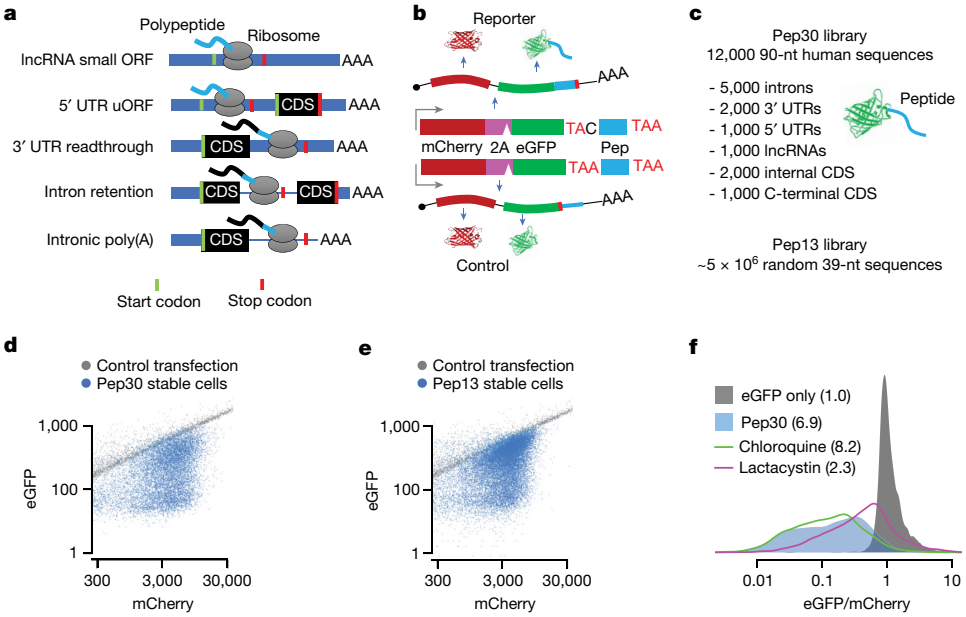

Fig. 1 | Noncoding translation products are unstable. a, Noncoding translation in diverse contexts generates a C-terminal tail derived from noncoding sequences. uORF, upstream open reading frame. **b**, Top, a mCherry-2A-eGFP bicistronic reporter for monitoring noncoding translation. Bottom, a control plasmid with a single base difference abolishing noncoding translation. Pep, noncoding sequence-derived peptide. **c**, Two cell libraries in which each cell stably expresses eGFP extended with either a sequence encoding up to 30 aa randomly selected from the human transcriptome (Pep30) or a random sequence encoding up to 13 aa (Pep13). **d**, Flow cytometry analysis of the Pep30 (**d**) or Pep13 (**e**) cell libraries. Also shown are cells transfected with the eGFP-only control reporter. **f**, Density plot of the eGFP/mCherry ratio for Pep30 stable cells without treatment or treated with the proteasome inhibitor lactacystin or the lysosome inhibitor chloroquine. Numbers in parentheses indicate the median fold loss of the eGFP/mCherry ratio of Pep30 reporters relative to the eGFP-only control.

fusing various noncoding sequences to the C-terminal end of the eGFP open reading frame (ORF) in an mCherry-2A-eGFP bicistronic reporter (Fig. 1b, top) and used the eGFP/mCherry ratio to quantify the effect of translation in noncoding sequences on the amount of eGFP in single cells while also normalizing for variations in transfection, transcription and translation rates[18,19]. As a control, we generated a similar plasmid with a single-nucleotide difference that creates a stop codon, preventing translation into the noncoding sequence (Fig. 1b, bottom). Using this reporter system in HEK 293T cells, we show that translation in the 3′ UTR of *HSP90B1*, the retained last intron of *GAPDH* and the prematurely polyadenylated intron 3 of *ACTB* all resulted in substantial loss of eGFP (9.5, 18.1 and 4.2-fold, respectively; Extended Data Fig. 1a,b). Inhibition of the proteasome but not the lysosome almost completely rescued the loss of eGFP caused by *ACTB* intron translation (1.4-fold loss of eGFP/mCherry ratio relative to control; Extended Data Fig. 1c), suggesting that the peptide encoded by the *ACTB* intron is degraded primarily by the proteasome.

To systematically investigate translation in diverse types of noncoding sequences, we generated a library of HEK 293T cells in which each cell stably expresses one of 12,000 bicistronic reporters, with eGFP fused to a C-terminal peptide encoded by an endogenous 90-nucleotide (nt) sequence randomly selected from human 5′ UTRs, 3′ UTRs, introns and lncRNAs, as well as canonical coding sequences (CDS) from both internal and terminal coding exons (Pep30 library; Fig. 1c; sequences are listed in Supplementary Table 2 and diversity is shown in Extended Data Fig. 2a). Using flow cytometry analysis, we observed a substantial loss of eGFP for almost all reporters, with no significant change in mCherry (Fig. 1d, median 6.9-fold decrease of eGFP/mCherry). These results suggest that translation in most noncoding sequences causes a decrease in the accumulation of the protein without affecting mRNA abundance. Six representative noncoding sequences were further tested with two non-eGFP reporters (RPL3 and PspCas13b) to rule out effects specific to eGFP or flow cytometry (Extended Data Fig. 1d–f).

We also generated a second library (Pep13) in which eGFP was fused to around 5 million random sequences of 39 nucleotides (encoding peptides up to 13 amino acids (aa)) and observed a similar loss of eGFP (Fig. 1e), suggesting that translation in 'unevolved' sequences is mitigated by default. Similar to the *ACTB* intron reporter (Extended Data Fig. 1c), the 6.9-fold loss of eGFP in the Pep30 cell library was reduced to 2.3-fold after 24 h of proteasome inhibition (lactacystin), with lysosome inhibition (chloroquine) having minimal effect (Fig. 1f; other inhibitors are shown in Extended Data Fig. 2b–d). These results demonstrate that aberrant translation products derived from diverse noncoding sequences are degraded primarily by the proteasome in human cells.

Instability linked to a hydrophobic C terminus

To quantify the expression of each reporter, we sorted cells with high eGFP and low eGFP expression into separate bins and sequenced the library DNA in each bin (Fig. 2a). Using the $\log_2$ ratio of read counts (eGFP high/eGFP low) as a measurement of eGFP expression (Fig. 2a), we found that eGFP expression is negatively correlated with the length of the tail peptide (peptides can be shorter than 30 aa owing to in-frame stop codons), with most peptides of 15 aa or more being associated with low eGFP expression (Fig. 2b). The strong dependence on tail peptide length, and therefore stop codon recognition, indicates that the loss of eGFP is largely owing to translation of the noncoding sequence, ruling out a major contribution of translation-independent mechanisms such as RNA degradation or sequestration mediated by the noncoding sequence.

To understand the determinants of degradation beyond the length of the tail peptide, we next focused on peptides of identical length (30 aa, $n = 4{,}726$). We found that translation in all classes of noncoding sequence is often associated with low protein expression, with the strongest effect observed in introns, followed by 3′ UTRs, lncRNAs and 5′ UTRs (Fig. 2c). Notably, internal CDS, regardless of whether they are

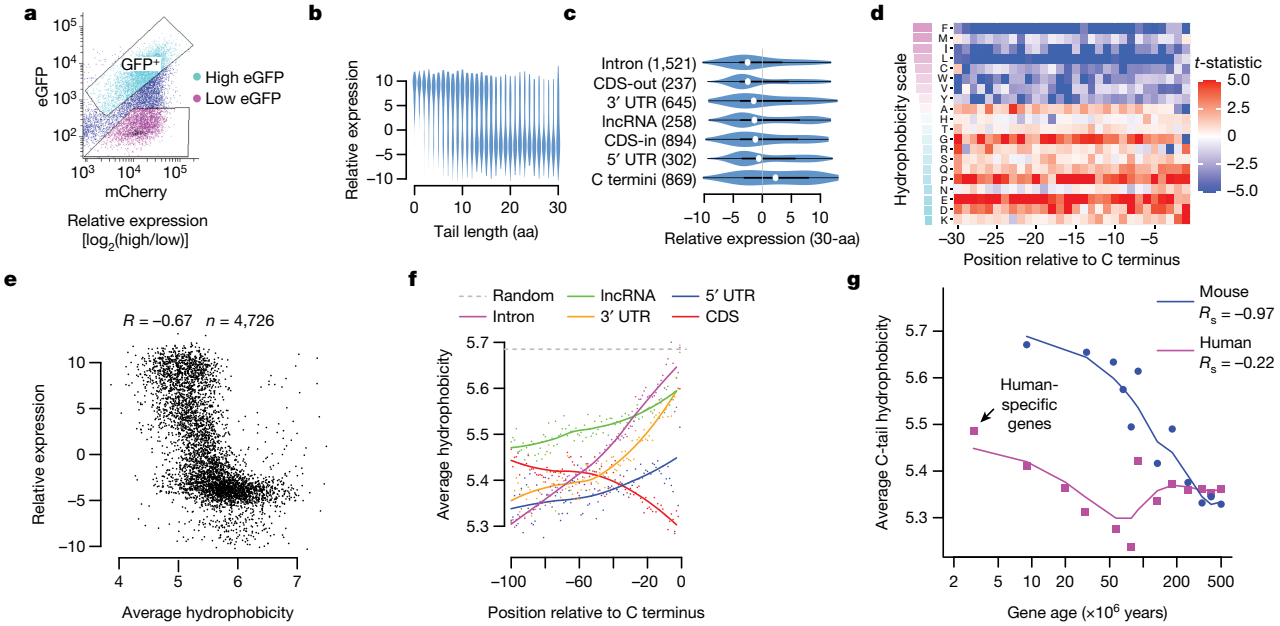

Fig. 2 | Noncoding translation mitigation is associated with C-terminal hydrophobicity. a, Pep30 stable cells were sorted into high-eGFP and low-eGFP bins and the tail-encoding DNA sequences were cloned and sequenced. The relative expression of each sequence is calculated as the $\log_2$ ratio of read counts in eGFP-high versus eGFP-low bins. **b**, Violin plots of relative expression for tails of varying lengths. **c**, Violin and box plots comparing the expression of 30-aa tails encoded by various types of sequences. The white dot indicates the median value, box edges delineate the top and bottom quartiles and whiskers extend to maximum and minimum values. The number of sequences in each category is shown in parentheses. CDS-out, frameshifted CDS; CDS-in, in-frame CDS. **d**, A heat map visualizing the association (two-sided Student's *t*-test statistics capped at 5.0) between expression and the presence of each amino acid at every position in the Pep30 library. Amino acids (rows) are sorted by hydrophobicity (Miyazawa scale). **e**, Average hydrophobicity versus relative expression for 30-aa tails. **f**, Genome-scale average hydrophobicity at each residue within the last 100 amino acids of peptides encoded by coding (at least 200 aa) and various noncoding sequences (at least 30 aa). **g**, Average C-tail (last 30 aa) hydrophobicity of human and mouse genes grouped by age based on the time of origination estimated from vertebrate phylogeny. The lines are a LOESS fit of the dots.

fused to eGFP in frame or out of frame, often resulted in low expression similar to that of noncoding sequences (Fig. 2c, CDS-in and CDS-out), with frameshifted CDS being more destabilizing than those preserving the reading frame. By contrast, endogenous C-terminal CDS, which are fused to eGFP in frame, comprise the only group that is more associated with high protein expression (Fig. 2c, C termini). These results indicate that the signal that triggers proteasomal degradation of aberrant translation products is also present in annotated CDS (albeit weaker) but is depleted from the C-terminal ends of annotated proteins. Our data thus underscore the importance of protein C termini in mediating protein degradation and suggest that functional proteins may have evolved to avoid proteasomal degradation, whereas proteins carrying an 'unevolved' C-terminal tail are degraded by default, as is the case with truncated proteins as well as peptides derived from noncoding sequences and random sequences.

To uncover the exact nature of the degradation signal, we next examined the amino acid composition and various physicochemical and structural properties of the tail peptides. Of note, almost all hydrophobic residues are associated with low eGFP expression at most positions in the 30-aa tail (Fig. 2d). The only exception is alanine, which is the least hydrophobic of the nine hydrophobic residues and is associated with low expression only at the last two positions, consistent with its function as a C-terminal end degron (C-degron) recognized by cullin-RING E3 ubiquitin ligases[31,32]. We also confirmed two other C-degrons, arginine at the 3rd from last position and glycine at the last position[31,32] (Fig. 2d). However, a 30-variable regression model using alanine, glycine and arginine residues in the last ten positions is only weakly predictive of eGFP expression (Spearman correlation coefficient (R_s) = −0.22). By contrast, the average hydrophobicity (Miyazawa scale) of residues in the 30-aa peptide has a much stronger negative correlation with eGFP expression (R_s = −0.67, Fig. 2e; similar results with other hydrophobicity scales are shown in Extended Data Fig. 3a).

Among all the physiochemical and structural properties that we examined, average hydrophobicity has the strongest negative correlation with expression (Extended Data Fig. 3b). Although several other properties, including transmembrane potential, also show a strong correlation with eGFP expression, these associations are largely owing to their correlation with hydrophobicity, as when controlling for hydrophobicity (partial correlation), most of these associations become much weaker (Extended Data Fig. 3b), but not vice versa. One prominent example is the tendency to be disordered (intrinsic disorder): although sometimes perceived as a trigger for protein degradation, protein disorder is positively correlated with eGFP expression (R_s = 0.65). However, this correlation was largely lost when controlling for hydrophobicity (R_s = 0.08). This is owing to a strong negative correlation between protein disorder and hydrophobicity[33] (R_s = −0.93). Similarly, peptides predicted to fold into either α-helices or β-sheets are associated with low expression, whereas peptides predicted to be unstructured (coil or loop) are more highly expressed. These results highlight the dominant role of C-terminal hydrophobicity, and not C-degrons or protein disorder, in triggering proteasomal degradation of polypeptides derived from diverse noncoding sequences in human cells.

Selection against C-terminal hydrophobicity

To determine whether C-terminal hydrophobicity underlies the aforementioned differential stability between canonical protein C termini and all other sequences, including internal protein sequences and peptides derived from noncoding sequences (Fig. 2c), we performed genome-wide in silico analysis of C-terminal hydrophobicity in the

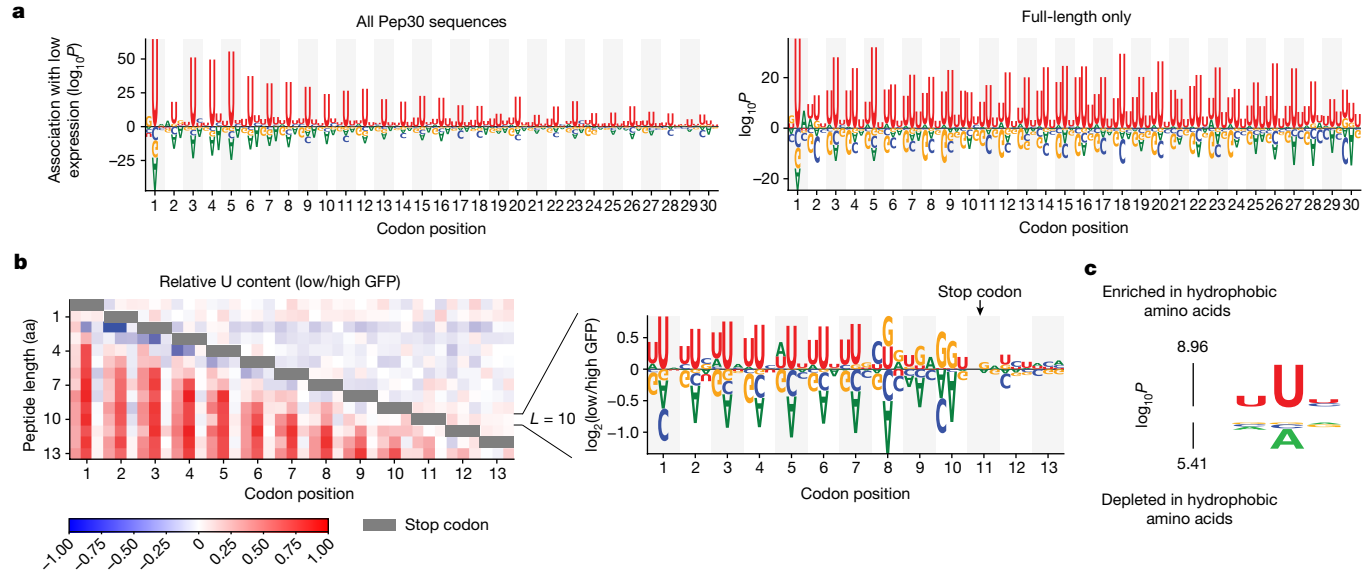

Fig. 3 | A bias in the genetic code links instability and hydrophobicity with U content. a, Nucleotides enriched or depleted in reporters of low eGFP expression in the Pep30 library using all sequences (left) or only sequences encoding a full-length 30-aa peptide (right). Height is scaled by $\log_{10}$ transformation of *P* values from two-sided Mann–Whitney *U* tests. **b**, A heat map colour-coding the $\log_2$ ratio of U frequency between Pep13 sequences in the GFP-low bin versus the GFP-high bin for each nucleotide and codon position and peptide length (*L*). Grey bars indicate positions of stop codons. The relative frequency of all four bases for $L = 10$ aa (stop codon at codon position 11) are shown on the right. **c**, Probability logo showing enriched and depleted nucleotides in codons of hydrophobic amino acids in the genetic code. *P* values were computed using two-sided Mann–Whitney *U* tests.

canonical proteome and the predicted noncoding proteome. We found that hydrophobic residues are progressively depleted towards the C-terminal end of canonical proteins (translated from CDS), especially within the last 30 amino acids, whereas the opposite trend is present for all other sequences (Fig. 2f). Notably, the extreme C termini of peptides from introns, 3′ UTRs, and lncRNAs have a hydrophobicity approaching that of entirely random amino acid sequences, suggesting that by default, unevolved nonfunctional proteins will have a relatively high average hydrophobicity and are subjected to proteasomal degradation. Similar results were obtained with a different hydrophobicity scale (Extended Data Fig. 3c). The depletion of C-terminal hydrophobicity is not detected at protein N termini (Extended Data Fig. 3d) and cannot be explained by the lack of protein domains near the C termini (Extended Data Fig. 3e).

Further supporting the evolutionary selection against protein C-terminal hydrophobicity, we found that in both humans and mice, evolutionarily young protein-coding genes tend to have higher hydrophobicity at the C-terminal tail (last 30 aa) than evolutionarily older genes (Fig. 2g). For example, human-specific genes—the youngest human genes originating after the human–chimpanzee divergence 4 to 6 million years ago[34]—have the highest C-terminal hydrophobicity as a group of all genes in the human genome. There is a strong negative correlation ($R_s = -0.97$, $P < 10^{-15}$) between estimated gene age and average protein C-tail hydrophobicity in the mouse genome, supporting the idea that as genes evolve, they progressively lose hydrophobic residues in the C-terminal tail, potentially resulting in longer protein half-lives. A similar, albeit weaker, trend is observed in the human genome, especially for genes originating within the past 100 million years (Fig. 2g).

Hydrophobicity bias in the genetic code

To understand why noncoding sequences tend to encode more hydrophobic amino acids, we examined the association between nucleotide composition and reporter expression in the Pep30 and Pep13 libraries. We observed a 3-nt periodicity of U enrichment in sequences associated with low eGFP expression in the Pep30 library, with U enrichment peaking at the centre position of each codon (Fig. 3a). There is a progressive decline of U bias from the 5′ to 3′ end, which disappears when sequences with premature in-frame stop codons are removed (Fig. 3a, right), suggesting that the 3-nt periodicity of U enrichment is translation-dependent. The dependence on the stop codon is more evident in the Pep13 library—the periodic enrichment of U ends 3 codons before the stop codon, and no significant nucleotide bias can be observed after the stop codon (Fig. 3b, more details in Extended Data Fig. 4a). The three codons immediately upstream of the stop codon are strongly enriched for codons encoding C-terminal degrons (Arg and Gly).

The association of low reporter expression with both hydrophobicity and U-rich codons suggests that hydrophobic amino acids are encoded by U-rich codons, especially with U at the centre position of the codon. This is indeed the case (Fig. 3c). In fact, all 16 codons with U at the centre position encode highly hydrophobic amino acids (Extended Data Fig. 4b). The strong reading frame-specific association of U content with hydrophobicity in the genetic code potentially contributes to the decreased stability of frameshifted CDS (Fig. 2c).

Although the association between U-rich codons and hydrophobic amino acids has been known since 1979[35], the biological importance remains unclear. Because canonical coding regions have evolved to be GC-rich and AT-poor relative to the AT-rich genomic background, sequences outside of functional coding regions are thus T-rich (U-rich after being transcribed into RNA) and tend to code for more hydrophobic residues. Indeed, we found a strong agreement between U content, C-terminal hydrophobicity and low reporter expression across different genomic regions. For example, introns have the highest U content (31.0%, Extended Data Fig. 4c), the highest C-terminal hydrophobicity (Fig. 2f), and the lowest reporter expression (Fig. 2c), whereas 5′ UTRs have a U content similar to that of coding regions and are also associated with moderate hydrophobicity. On average, amino acids coded by the AT-rich noncoding genome are 40% more likely to be hydrophobic (Phe, Met, Ile, Leu, Cys, Trp, Val or Tyr) than the last 30 amino acids at the C terminus of canonical proteins (37.7% versus 27.0%). Although the

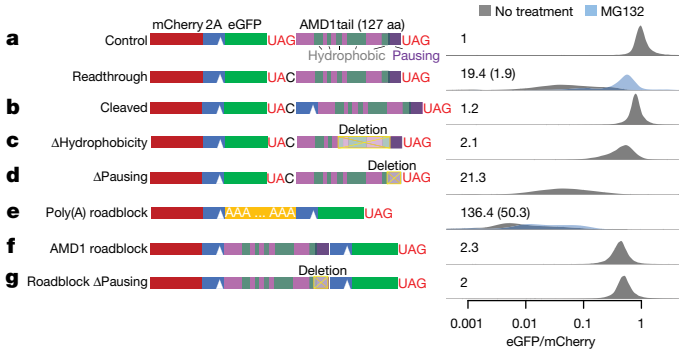

Fig. 4 | Mitigation of *AMD1* 3′ UTR translation. a–g, Reporter constructs shown on the left were transfected into HEK 293T cells. The eGFP/mCherry ratio was quantified in individual cells using flow cytometry with distributions shown on the right. The number in each plot is the median fold decrease of the eGFP/mCherry ratio. Data from cells treated with the proteasome inhibitor MG-132 are shown in parentheses. **a**, Control and readthrough. **b**, An extra 2A site cleaving the AMD1 tail peptide from eGFP. **c**, Deletion of C-terminal hydrophobic regions. **d**, Deletion of the ribosome pausing sequence. **e**, Insertion of a poly(A) sequence as a roadblock between mCherry and eGFP. **f**, Insertion of the AMD1 tail ORF as a roadblock. **g**, Insertion of the AMD1 tail ORF without the ribosome pausing sequence.

absolute difference is moderate for individual residues, the clustering of multiple hydrophobic residues—which scales exponentially with cluster size—is probably what triggers proteasomal degradation. For example, a 1.4-fold difference translates into a tenfold difference for a cluster of 7 hydrophobic residues.

Together, our massively parallel reporter assays and integrative genomic analysis support a unified model for the mitigation of translation in diverse noncoding sequences: noncoding sequences tend to have high U content and are therefore more likely to code for hydrophobic residues, resulting in a hydrophobic C terminus that triggers proteasomal degradation. Functional proteins, on the contrary, have evolved to deplete hydrophobic residues near the C termini.

Surveillance of *AMD1* 3′ UTR translation

Previously, ribosome stalling and not proteasomal degradation had been proposed to explain the surveillance of readthrough translation in the 3′ UTR of *AMD1*[16]. Ribosomes pause near the in-frame stop codon in the 3′ UTR, and the last 21 codons in the *AMD1* 3′ UTR ORF (Fig. 4a) have been found to be necessary to induce ribosome pausing in cell-free assays[16]. Ribosome pausing was proposed to result in a queue of stalled ribosomes covering the entire 3′ UTR, preventing further translation in the 3′ UTR[16]. However, no ribosome footprints indicative of a ribosome queue could be observed in the *AMD1* 3′ UTR[16,29].

In our reporter system, readthrough translation of the *AMD1* 3′ UTR led to a 19.4-fold decrease of eGFP/mCherry (Fig. 4a). Western blot analysis confirms the loss of eGFP protein, ruling out eGFP misfolding as the cause of reduced fluorescence in flow cytometry assays (Extended Data Fig. 5a). However, unlike the conclusion from the previous study[16], we found that proteasome inhibition by MG-132 almost completely rescued the decrease in eGFP/mCherry ratio (from 19.4-fold to 1.9-fold, Fig. 4a), similar to other reporters used in our study. Furthermore, eGFP can be almost completely stabilized by a P2A peptide that results in co-translational cleavage of the AMD1 peptide from eGFP (Fig. 4b), a rescue that cannot be explained by the ribosome queueing model. We identified multiple hydrophobic regions within the 127-aa AMD1 peptide that may serve as the degron (Fig. 4a). Whereas no rescue was observed when deleting individual hydrophobic regions (Extended Data Fig. 5b,c), a substantial rescue was observed when the three most C-terminal hydrophobic regions were deleted simultaneously while retaining most of the ribosome pausing signal (Fig. 4c). These results suggest that the hydrophobic regions act redundantly to mediate degradation of the AMD1 peptide.

Notably, deleting the ribosome pausing sequence (the last 21 codons) in the reporter did not rescue the loss of eGFP (Fig. 4d). To directly test whether the *AMD1* 3′ UTR sequence can act as a roadblock for ribosomes, we adapted a tricistronic reporter system previously used to assess ribosome stalling by a poly(A) sequence[36]. Specifically, a poly(A) sequence (A_{63}) inserted between mCherry and eGFP (separated by T2A and P2A) caused a 136-fold decrease of eGFP relative to mCherry that could not be rescued with proteasome inhibition (Fig. 4e), consistent with the model that ribosomes stall in the poly(A) region and thus cannot translate the downstream eGFP. By contrast, replacing A_{63} with the *AMD1* 3′ UTR ORF caused a decrease of only about twofold in eGFP (Fig. 4f), suggesting that unlike A_{63}, most ribosomes experience no difficulty translating through the *AMD1* 3′ UTR ORF. The twofold effect persists after deleting the 21-codon ribosome pausing signal (Fig. 4g, also see the replicate in Extended Data Fig. 6), suggesting this that effect is attributable to factors other than ribosome stalling, such as incomplete cleavage by T2A and/or ribosome fall-off after the T2A sequence[37]. Our results thus argue against the formation of a ribosome queue caused by stable ribosome stalling at the *AMD1* 3′ UTR ORF in cells.

Together, our results suggest that similar to other noncoding sequences, the reduced protein output from *AMD1* 3′ UTR translation is mainly caused by C-terminal hydrophobicity-mediated proteasomal degradation rather than ribosome queueing-mediated inhibition of translation elongation.

BAG6 mediates proteasomal degradation

To unravel the molecular pathway that captures noncoding sequence-derived peptides for proteasomal degradation, we performed a genome-wide CRISPR-knockout screen[38] using the *AMD1* readthrough reporter (Fig. 5a). The unbiased screen unambiguously supported the role of the proteasome: of the genes whose knockout resulted in a rescue (higher eGFP/mCherry ratio), most (17 out of 20) of the top hits (false discovery rate (FDR) < 0.01) are components of the 26S proteasome in the ubiquitin-dependent protein degradation pathway (Fig. 5b, red). By contrast, none of the genes that are known to be involved in resolving ribosome stalling, such as the RQC factors *NEMF* and *LTN1*, have any effect on the eGFP/mCherry ratio (Fig. 5b, green), again arguing against the role of ribosome stalling and queueing in the mitigation of *AMD1* 3′ UTR translation. Similarly, knockout of lysosomal genes has no effect on the eGFP/mCherry ratio (Supplementary Table 3).

Of note, the remaining three top hits with FDR < 0.01, *BAG6*, *TRC35* (also known as *GET4*), and *RNF126*, are all key components of the highly conserved BAG6 pathway for membrane protein triage in the cytosol[39–42] (Fig. 5c). The BAG6 pathway is embedded as a quality control module in the transmembrane domain recognition complex (TRC) pathway (also known as the guided entry of tail-anchored proteins (GET) pathway), for the triage of tail-anchored membrane proteins. Tail-anchored proteins have a hydrophobic C-terminal tail that functions as a transmembrane domain and also serves as the membrane-targeting signal. Immediately after being released from the ribosome, tail-anchored proteins are captured by the ribosome-associated co-chaperone SGTA, which binds and shields the hydrophobic transmembrane domain in nascent tail-anchored proteins[39–41]. SGTA then delivers the substrate to the BAG6–UBL4A–TRC35 heterotrimeric complex via binding to UBL4A. Authentic tail-anchored proteins are transferred directly from SGTA to TRC40, which is associated with the trimeric complex via TRC35, and are then committed to membrane targeting. Defective tail-anchored

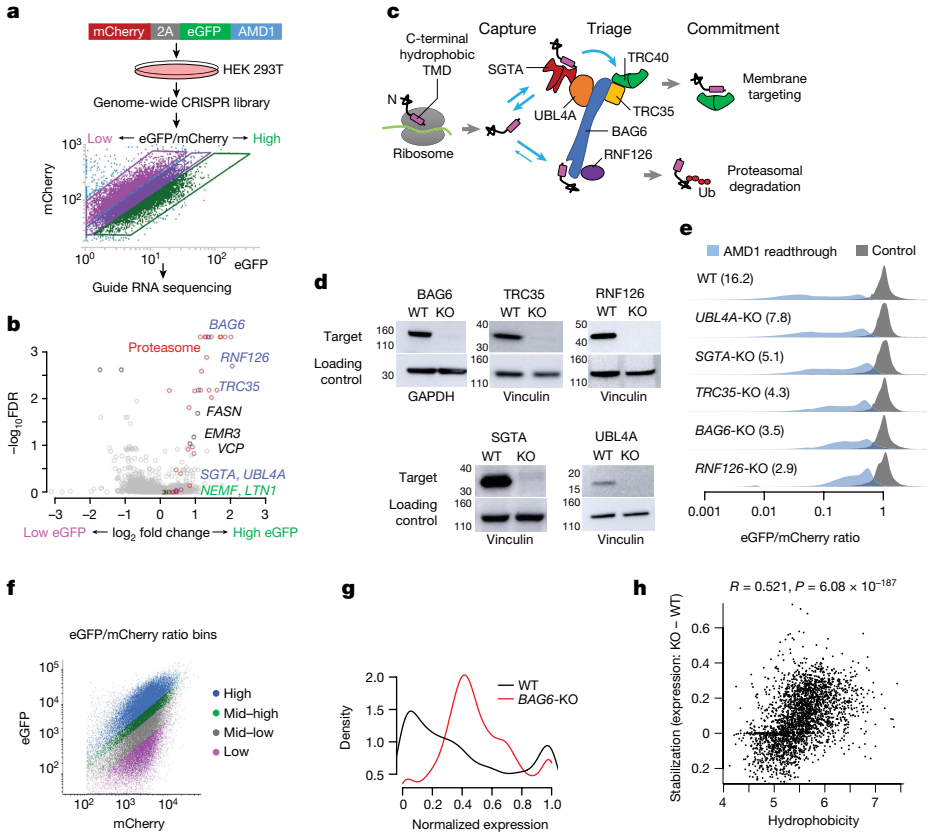

Fig. 5 | The BAG6 pathway mediates proteasomal degradation of noncoding translation products. a, A CRISPR screen using the AMD1 reporter stably integrated into HEK 293T cells. **b**, Gene-level summary of the CRISPR screen from MAGeCK. **c**, Schematic of the BAG6 pathway, which targets proteins with a C-terminal hydrophobic region. TMD, transmembrane domain; Ub, ubiquitin. **d**, Representative western blots confirming the depletion of proteins in the corresponding knockout cells ($n = 2$ biologically independent samples). GAPDH was used as loading control for BAG6 and vinculin was used for all other proteins. WT, wild type. **e**, eGFP/mCherry ratio of the AMD1 reporter in wild-type and knockout cells ($n = 1$). The numbers in parentheses are the median fold decrease of the eGFP/mCherry ratio in the readthrough reporter relative to the control. **f**, Wild-type and *BAG6*-KO HEK 293T cells were transduced with the Pep30 library and sorted into four bins according to eGFP/mCherry ratio and then sequenced. **g**, Density plot of normalized expression of each sequence in wild-type and *BAG6*-KO cells. **h**, Scatter plot of stabilization versus average hydrophobicity of each tail peptide. Shown are the Spearman correlation coefficient *R* and the *P* value from a two-sided Spearman's correlation test. No adjustments were made for multiple comparisons.

proteins, however, are released from SGTA and re-captured by BAG6, which recruits the E3 ubiquitin ligase RNF126 that catalyses the ubiquitination of the substrate, committing it to proteasomal degradation[43,44]. In addition to acting as an adapter for TRC40 in the membrane-targeting arm of the pathway, TRC35 also blocks the nuclear localization signal on BAG6 and retains BAG6 in the cytosol for protein quality control[45].

Three features of the BAG6 pathway make it especially appealing for the surveillance of translation in noncoding sequences. First, the pathway recognizes C-terminal hydrophobic tails, a defining feature of aberrant translation products that is also associated with their degradation (Fig. 2). Second, multiple components of this pathway, including BAG6, TRC35 and SGTA are physically associated with translating ribosomes[41,42,46], positioning the complex for rapid surveillance of aberrant translation products before they are released to the cytoplasm. Last, the BAG6 complex functions at the intersection of membrane targeting and proteasomal degradation, potentially explaining why most evolutionarily young proteins derived from noncoding sequences are preferentially localized to membranes (Supplementary Table 1).

We used CRISPR–Cas9 to generate clonal knockout HEK 293T cell lines for the 3 top hits *BAG6*, *RNF126* and *TRC35*, as well as for *SGTA* and *UBL4A*, which were upstream of BAG6 in the pathway but missed by the CRISPR screen (Fig. 5d and Extended Data Fig. 7a). Substantial rescue of the *AMD1* readthrough reporter was observed in all knockout cell lines with the strongest rescue in *RNF126*-KO and *BAG6*-KO cells (Fig. 5e). The partial rescue in *SGTA*-KO and *UBL4A*-KO cells suggests that *SGTA* and *UBL4A* were probably false negatives in the CRISPR screen, possibly owing to low guide RNA efficiencies. Transient re-expression of wild-type BAG6 or RNF126 but not the corresponding mutant forms partially reversed the knockout phenotype on the *AMD1* reporter (Extended Data Fig. 7b,c). *BAG6*-KO and *RNF126*-KO cells are viable but grow significantly slower than wild-type cells in a co-culture assay (Extended Data Fig. 7d,e). Proteasome assembly and activity are not affected in the knockout cells (Extended Data Fig. 8), ruling out the alternative model that BAG6 indirectly affects reporter level via its impact on proteasome assembly[47]. BAG6 co-immunoprecipitated with the eGFP–AMD1 fusion protein, an association that was almost completely lost when the hydrophobic region required for degradation was deleted (Extended Data Fig. 5d). Together, our genetic and biochemical analyses of the *AMD1* reporter support a model in which BAG6 binds to C-terminal hydrophobic regions in substrates and results in proteasomal degradation.

To systematically test the role of BAG6 in mediating the proteasomal degradation of aberrant translation products from diverse noncoding sequences beyond the AMD1 tail, we repeated the Pep30 high-throughput reporter assay in both wild-type and *BAG6*-KO cells (Fig. 5f). To increase the sensitivity of the assay, we sorted cells into four bins on the basis of their eGFP/mCherry ratio and calculated a normalized expression value for each sequence using read counts in

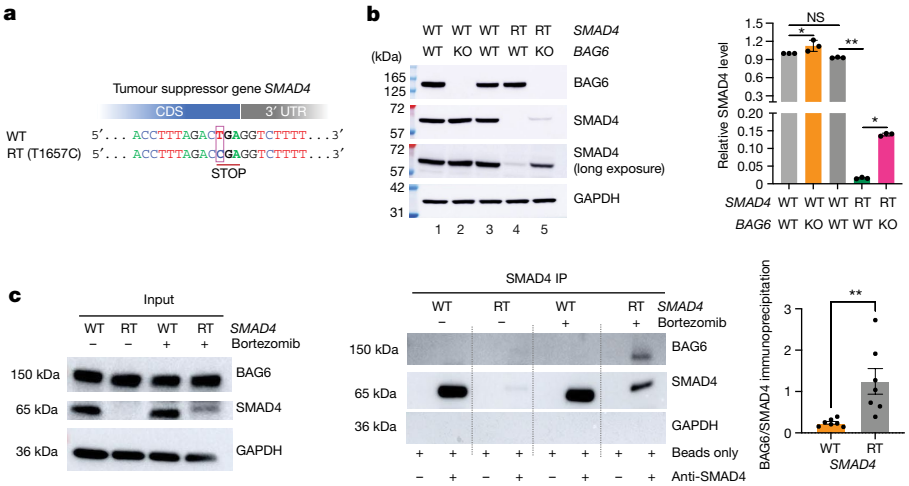

Fig. 6 | SMAD4 readthrough protein as an endogenous substrate of BAG6. **a**, The mutation T1657C disrupts the *SMAD4* stop codon and results in readthrough (RT) translation in the 3′ UTR. **b**, Left, the SMAD4 readthrough protein is barely detectable in *BAG6* wild-type cells (lane 4) but is stabilized in *BAG6*-KO cells (lane 5). Lane 1, parental wild-type cells for *BAG6*-KO. Lane 3, parental wild-type cells for *SMAD4* readthrough. Right, quantification of SMAD4 from the blot. $n = 3$ biologically independent samples. Data are mean ± s.d. **c**, BAG6 co-immunoprecipitates with SMAD4 readthrough products. Bortezomib is a proteasome inhibitor. $n = 7$ biologically independent samples. Data are mean ± s.d. Two-sided Student's *t*-test, no adjustments were made for multiple comparisons. $^{*}P < 0.05$, $^{**}P < 0.01$. NS, not significant.

the sorted bins (Methods). A large fraction of the sequences showed an increase of expression in *BAG6*-KO cells (Fig. 5g), indicating that BAG6 mediates the degradation of many noncoding translation products. Notably, the extent of rescue by *BAG6*-KO is correlated with the average hydrophobicity of the tail sequence (Fig. 5h, $R = 0.52$, $P = 2 \times 10^{-187}$), consistent with a model in which BAG6 binds hydrophobic C-terminal tails and mediates proteasomal degradation. The results in Fig. 5g,h were validated in a biological replicate (Extended Data Fig. 9).

In sum, our genome-wide screen and systematic follow-up validations uncovered an unexpected role of the BAG6 membrane protein triage pathway in mediating proteasomal degradation of diverse non-canonical ORF translation products.

Cancer mutants as endogenous substrates

Recurrent mutations identified from the COSMIC cancer mutation database disrupt the stop codons of more than 400 cancer-associated genes resulting in translation into their 3′ UTRs, including in the tumour suppressor gene *SMAD4*[10] (Fig. 6a). Consistent with our model, the *SMAD4* 3′ UTR encodes a short hydrophobic sequence that leads to proteasomal degradation of the *SMAD4* readthrough product[10]. Using our dual-colour reporter system, we confirmed that fusing *SMAD4* 3′ UTR encoded peptide to eGFP resulted in a substantial (20.5-fold) loss of eGFP fluorescence, which was partially rescued in *BAG6*-KO cells (Extended Data Fig. 10a). Using a previously generated HEK 293T cell line carrying a homozygous *SMAD4* readthrough mutation T1657C[10], we confirmed that the endogenous SMAD4 readthrough protein is almost completely degraded (Fig. 6b, lane 4). We further derived a clonal *BAG6*-KO cell line from the *SMAD4* T1657C readthrough cell line and found that the endogenous SMAD4 readthrough protein can be stabilized by *BAG6* knockout (Fig. 6b, lane 5) without an increase of *SMAD4* mRNA abundance (Extended Data Fig. 10b). Depleting RNF126 similarly resulted in a rescue of the reporter and endogenous SMAD4 readthrough (Extended Data Fig. 10). BAG6 was co-immunoprecipitated with endogenous SMAD4 readthrough protein but not wild-type SMAD4, despite the wild-type protein being much more abundant (Fig. 6c). Together, these results show that in addition to exogenously expressed reporters, the BAG6 pathway also mediates the degradation of endogenous readthrough proteins, such as SMAD4 readthrough via binding to the 3′ UTR coded hydrophobic C-terminal tail. Our results uncover details of a new mechanism for how tumour suppressor genes are inactivated in cancer.

Discussion

We combined massively parallel reporter assays, genome-wide CRISPR screens, integrative genomic analysis and in-depth genetic and biochemical dissections to uncover a mechanism underlying the surveillance of widespread translation in diverse noncoding sequences in human cells. Noncoding sequences such as lncRNAs, 5′ UTRs, 3′ UTRs and introns are heterogeneous in biogenesis, sequence and structure. It has so far remained unclear whether a common mechanism is used for the surveillance of translation of such diverse sequences. Our data suggest that there are at least two common features: compositional bias (U richness or hydrophobicity) and positional bias (C termini), that together distinguish polypeptides translated from noncoding sequences to those translated from functional coding sequences.

Proteasomal degradation of intracellular proteins generates short peptides that are presented as antigens on major histocompatibility complex class I (MHCI) on the surface of almost all animal cells. Antigen presentation enables T cells to detect cancer cells and cells infected by viruses. It has been proposed that up to 30% of newly synthesized proteins are rapidly degraded and presented on MHCI complexes, enabling the rapid detection of viral infections[48]. The nature of these short-lived defective ribosomal products and how their rapid degradation is triggered remain unknown. A previous study has shown that BAG6 is associated with newly synthesized poly-ubiquitinated polypeptides and that BAG6 knockdown impairs MHCI antigen presentation[49], implicating BAG6 substrates as a source of rapidly presented antigens. By uncovering diverse noncoding translation products as BAG6 substrates, our results suggest that BAG6-mediated degradation of noncoding translation products provides an important source of antigens and potentially underlies the dominance of noncoding sequence-derived peptides among tumour-specific antigens. Our results are also consistent with a previous study suggesting hydrophobicity as a driver of MHCI antigen processing[50]. The BAG6 pathway thus represents a potential node of regulation and drug target for tuning the visibility of cancer cells to the immune system.

The unexpected finding that polypeptides translated from noncoding sequences are fed into a membrane protein biogenesis and triage pathway has important implications for understanding the impact of aberrant translation on cell functions and gene evolution. This raises the possibility that the influx from aberrant translation may interfere with the biogenesis and quality control of tail-anchored proteins, especially in the context of cancer, neurodegeneration and ageing, where there is a global increase in aberrant translation. On the evolutionary timescale, in addition to lncRNA-derived peptides, alternative splicing and polyadenylation isoforms of known coding genes may also evolve new functions on membranes, enabling specializations of existing functions on membranes. The BAG6 pathway may have a key role in balancing protein quality control over physiological timescales and innovation of new proteins over evolutionary timescales.

In addition to the BAG6 pathway that we have validated, our genome-wide screen also suggests potential alternative mechanisms for the surveillance of translation in noncoding sequences. These alternative mechanisms, potentially activated in the absence of the BAG6 pathway in knockout cells, may explain the partial rescue of *AMD1* and *SMAD4* readthrough translation and the existence of Pep30 sequences that are insensitive to *BAG6* knockout. We envision that the resources generated here, including the CRISPR screen, BAG6-independent Pep30 sequences and knockout cell lines will facilitate future studies in uncovering mechanisms for the surveillance of translation in noncoding sequences.

Online content

Any methods, additional references, Nature Portfolio reporting summaries, source data, extended data, supplementary information, acknowledgements, peer review information; details of author contributions and competing interests; and statements of data and code availability are available at https://doi.org/10.1038/s41586-023-05946-4.

1. Ingolia, N. T. et al. Ribosome profiling reveals pervasive translation outside of annotated protein-coding genes. *Cell Rep.* **8**, 1365–1379 (2014).
2. Ji, Z., Song, R., Regev, A. & Struhl, K. Many lncRNAs, 5′UTRs, and pseudogenes are translated and some are likely to express functional proteins. *eLife* **4**, e08890 (2015).
3. Weatheritt, R. J., Sterne-Weiler, T. & Blencowe, B. J. The ribosome-engaged landscape of alternative splicing. *Nat. Struct. Mol. Biol.* **23**, 1117–1123 (2016).
4. Sudmant, P. H., Lee, H., Dominguez, D., Heiman, M. & Burge, C. B. Widespread accumulation of ribosome-associated isolated 3′ UTRs in neuronal cell populations of the aging brain. *Cell Rep.* **25**, 2447–2456 e2444 (2018).
5. Adusumalli, S., Ngian, Z. K., Lin, W. Q., Benoukraf, T. & Ong, C. T. Increased intron retention is a post-transcriptional signature associated with progressive aging and Alzheimer's disease. *Aging Cell* **18**, e12928 (2019).
6. Mazin, P. et al. Widespread splicing changes in human brain development and aging. *Mol. Syst. Biol.* **9**, 633 (2013).
7. Hsieh, Y. C. et al. Tau-mediated disruption of the spliceosome triggers cryptic RNA splicing and neurodegeneration in Alzheimer's disease. *Cell Rep.* **29**, 301–316.e310 (2019).
8. Dvinge, H. & Bradley, R. K. Widespread intron retention diversifies most cancer transcriptomes. *Genome Med.* **7**, 45 (2015).
9. Lee, S. H. et al. Widespread intronic polyadenylation inactivates tumour suppressor genes in leukaemia. *Nature* **561**, 127–131 (2018).
10. Dhamija, S. et al. A pan-cancer analysis reveals nonstop extension mutations causing SMAD4 tumour suppressor degradation. *Nat. Cell Biol.* **22**, 999–1010 (2020).
11. Laumont, C. M. et al. Noncoding regions are the main source of targetable tumor-specific antigens. *Sci. Transl. Med.* **10**, eaau5516 (2018).
12. Xiang, R. et al. Increased expression of peptides from non-coding genes in cancer proteomics datasets suggests potential tumor neoantigens. *Commun. Biol.* **4**, 496 (2021).
13. Smart, A. C. et al. Intron retention is a source of neoepitopes in cancer. *Nat. Biotechnol.* **36**, 1056–1058 (2018).
14. Vakirlis, N. et al. De novo emergence of adaptive membrane proteins from thymine-rich genomic sequences. *Nat. Commun.* **11**, 781 (2020).
15. Carvunis, A. R. et al. Proto-genes and de novo gene birth. *Nature* **487**, 370–374 (2012).
16. Yordanova, M. M. et al. AMD1 mRNA employs ribosome stalling as a mechanism for molecular memory formation. *Nature* **553**, 356–360 (2018).
17. Hashimoto, S., Nobuta, R., Izawa, T. & Inada, T. Translation arrest as a protein quality control system for aberrant translation of the 3′-UTR in mammalian cells. *FEBS Lett.* **593**, 777–787 (2019).
18. Arribere, J. A. et al. Translation readthrough mitigation. *Nature* **534**, 719–723 (2016).
19. Kramarski, L. & Arbely, E. Translational read-through promotes aggregation and shapes stop codon identity. *Nucleic Acids Res.* **48**, 3747–3760 (2020).
20. Chen, J. et al. Pervasive functional translation of noncanonical human open reading frames. *Science* **367**, 1140–1146 (2020).
21. van Heesch, S. et al. The translational landscape of the human heart. *Cell* **178**, 242–260. e229 (2019).
22. Djebali, S. et al. Landscape of transcription in human cells. *Nature* **489**, 101–108 (2012).
23. Bai, B. et al. U1 small nuclear ribonucleoprotein complex and RNA splicing alterations in Alzheimer's disease. *Proc. Natl Acad. Sci. USA* **110**, 16562–16567 (2013).
24. Wang, L. et al. SF3B1 and other novel cancer genes in chronic lymphocytic leukemia. *N. Engl. J. Med.* **365**, 2497–2506 (2011).
25. Hsu, T. Y. et al. The spliceosome is a therapeutic vulnerability in MYC-driven cancer. *Nature* **525**, 384–388 (2015).
26. Wang, D. et al. Inhibition of nonsense-mediated RNA decay by the tumor microenvironment promotes tumorigenesis. *Mol. Cell. Biol.* **31**, 3670–3680 (2011).
27. Son, H. G. et al. RNA surveillance via nonsense-mediated mRNA decay is crucial for longevity in *daf-2*/insulin/IGF-1 mutant *C. elegans*. *Nat. Commun.* **8**, 14749 (2017).
28. Sun, Y., Eshov, A., Zhou, J., Isiktas, A. U. & Guo, J. U. C9orf72 arginine-rich dipeptide repeats inhibit UPF1-mediated RNA decay via translational repression. *Nat. Commun.* **11**, 3354 (2020).
29. Wangen, J. R. & Green, R. Stop codon context influences genome-wide stimulation of termination codon readthrough by aminoglycosides. *eLife* **9**, e52611 (2020).
30. Dong, C. et al. Intron retention-induced neoantigen load correlates with unfavorable prognosis in multiple myeloma. *Oncogene* **40**, 6130–6138 (2021).
31. Lin, H. C. et al. C-terminal end-directed protein elimination by CRL2 ubiquitin ligases. *Mol. Cell* **70**, 602–613.e603 (2018).
32. Koren, I. et al. The eukaryotic proteome is shaped by E3 ubiquitin ligases targeting C-terminal degrons. *Cell* **173**, 1622–1635.e1614 (2018).
33. Dyson, H. J. & Wright, P. E. Intrinsically unstructured proteins and their functions. *Nat. Rev. Mol. Cell Biol.* **6**, 197–208 (2005).
34. Zhang, Y. E., Vibranovski, M. D., Landback, P., Marais, G. A. B. & Long, M. Y. Chromosomal redistribution of male-biased genes in mammalian evolution with two bursts of gene gain on the X chromosome. *PLoS Biol.* **8**, e1000494 (2010).
35. Wolfenden, R. V., Cullis, P. M. & Southgate, C. C. Water, protein folding, and the genetic code. *Science* **206**, 575–577 (1979).
36. Juszkiewicz, S. & Hegde, R. S. Initiation of quality control during poly(A) translation requires site-specific ribosome ubiquitination. *Mol. Cell* **65**, 743–750 e744 (2017).
37. Liu, Z. et al. Systematic comparison of 2A peptides for cloning multi-genes in a polycistronic vector. *Sci Rep.* **7**, 2193 (2017).
38. Wang, T., Wei, J. J., Sabatini, D. M. & Lander, E. S. Genetic screens in human cells using the CRISPR–Cas9 system. *Science* **343**, 80–84 (2014).
39. Wunderley, L., Leznicki, P., Payapilly, A. & High, S. SGTA regulates the cytosolic quality control of hydrophobic substrates. *J. Cell Sci.* **127**, 4728–4739 (2014).
40. Shao, S., Rodrigo-Brenni, M. C., Kivlen, M. H. & Hegde, R. S. Mechanistic basis for a molecular triage reaction. *Science* **355**, 298–302 (2017).
41. Hessa, T. et al. Protein targeting and degradation are coupled for elimination of mislocalized proteins. *Nature* **475**, 394–397 (2011).
42. Mariappan, M. et al. A ribosome-associating factor chaperones tail-anchored membrane proteins. *Nature* **466**, 1120–1124 (2010).
43. Rodrigo-Brenni, M. C., Gutierrez, E. & Hegde, R. S. Cytosolic quality control of mislocalized proteins requires RNF126 recruitment to Bag6. *Mol. Cell* **55**, 227–237 (2014).
44. Hu, X. et al. RNF126-mediated reubiquitination is required for proteasomal degradation of p97-extracted membrane proteins. *Mol. Cell* **79**, 320–331.e329 (2020).
45. Wang, Q. et al. A ubiquitin ligase-associated chaperone holdase maintains polypeptides in soluble states for proteasome degradation. *Mol. Cell* **42**, 758–770 (2011).
46. Leznicki, P. & High, S. SGTA associates with nascent membrane protein precursors. *EMBO Rep.* **21**, e48835 (2020).
47. Akahane, T., Sahara, K., Yashiroda, H., Tanaka, K. & Murata, S. Involvement of Bag6 and the TRC pathway in proteasome assembly. *Nat. Commun.* **4**, 2234 (2013).
48. Yewdell, J. W. & Nicchitta, C. V. The DRiP hypothesis decennial: support, controversy, refinement and extension. *Trends Immunol.* **27**, 368–373 (2006).
49. Minami, R. et al. BAG-6 is essential for selective elimination of defective proteasomal substrates. *J. Cell Biol.* **190**, 637–650 (2010).
50. Huang, L., Kuhls, M. C. & Eisenlohr, L. C. Hydrophobicity as a driver of MHC class I antigen processing. *EMBO J.* **30**, 1634–1644 (2011).

Methods

Plasmids

HSP90B1, *ACTB*, *GAPDH* and *SMAD4* reporters: the 3′ UTR of *HSP90B1*, intron 3 of *ACTB*, the last intron of *GAPDH* and the 3′ UTR of *SMAD4* were amplified by PCR from the genomic DNA of HEK 293T cells with the primers listed in Supplementary Table 4. The PCR products were then either digested with NotI and SbfI (*GAPDH* and *SMAD4*) or with NsiI-HF and PspOMI (*ACTB* and *HSP90B1*), which generate the same overhangs. The inserts were then ligated with NotI- and SbfI-digested pJA291 (Addgene #74487)[18].

***AMD1* reporters.** The *AMD1* readthrough reporter was generated by inserting genomic DNA-amplified fragment into pJA291 using NotI and SbfI sites. Overlap extension PCR (OEP) cloning was used to insert a P2A sequence between eGFP and the AMD1 tail in the readthrough reporter. Systematic deletion of individual or combinations of hydrophobic regions from the readthrough reporter were done using NEB Q5 Site-Directed Mutagenesis (SDM) Kit (E0554). The *AMD1* roadblock reporter was generated using OEP cloning. OEP cloning was again used to delete the putative ribosome pausing signal from the roadblock reporter or replace the *AMD1* sequence with a poly(A) sequence or the *XBP1* stalling sequence. Deletion of the ribosome stalling signal from the readthrough reporter was also generated by OEP cloning. XBP1 stalling sequence was amplified from Addgene plasmid #159583 with Phusion PCR kit (New England Biolabs, M0530S).

Representative noncoding sequence reporters. Six noncoding sequences from the Pep30 library (*KRT2* intron, *APOL4* intron, *ASPAY* 3′ UTR, *IFT81* 3′ UTR, *LINC00222* and *LINC02885*) were selected and cloned into either the original mCherry-eGFP bicistronic Pep30 reporter, fused to the C-terminal of HA-tagged dPspCas13b protein (Addgene plasmid #103866), or fused to the C-terminal of human ribosomal protein L3 (*RPL3*). The noncoding sequences were amplified from the Pep30 library with primer pairs carrying restriction site pairs to be used for cloning. The following pairs of restriction sites were used for each of the three reporter backbones: NotI and SbfI for mCherry/eGFP bicistronic reporter pJA291, and AscI and EcoRI for both dPspCas13b and RPL3 reporters.

CRISPR guide RNA plasmids. The parental lentiCRISPR v2 plasmid (Addgene #52961) was digested with BsmBI and purified using the NucleoSpin Gel and PCR Clean-up kit (Macherey-Nagel). Forward and reverse oligonucleotides containing the guide sequence of interest were phosphorylated and annealed and ligated into the parental plasmid with T4 PNK and T4 DNA ligase. Targeting and non-targeting guide sequences are derived from the CRISPR-KO library described previously[38].

All plasmids were transformed into NEB Stable Competent *Escherichia coli* (C3040) according to the manufacturer's protocol. Positive clones were confirmed via sanger sequencing. All primers used for cloning and sanger sequencing are listed in Supplementary Table 4.

Cell culture

HEK 293T cells used in this study were purchased from ATCC and have not been authenticated by our laboratory. Cells were cultured in DMEM with 4.5 g l^{-1} D-glucose supplemented with 10% fetal bovine serum, 1% penicillin/streptomycin was added except when producing lentivirus. Low passage number cells were used and maintained under 90% visual confluency. Cells were maintained at 5% CO_2 and 37 °C. HEK 293T cells used in this study were confirmed to be negative for mycoplasma contamination and routinely tested using the MycoAlert Mycoplasma Detection Kit (Lonza, LT07-418). For experiments involving the *SMAD4* gene, clonal cell lines harbouring *SMAD4* readthrough mutations as well as the parental HEK 293T cells were obtained as a gift from S. Diederichs. Transfection of plasmids was done using Lipofectamine 2000 or Lipofectamine 3000 according to the manufacturer's instructions. Flow cytometry analyses of transfected cells were typically performed 24 or 48 h after transfection.

RNF126 knockdown

HEK 293T cells were seeded in 6-well plate with 2.5×10^5 cells per well. Cells were transfected the next day with either 25 pmol siControl (Horizon Discovery, D-001810-10-05) or 25 pmol siRNF126 (Horizon Discovery, L-007015-00-0005) using lipofectamine RNAiMAX. Target sequences of the siRNA *RNF126*-targeting pool are as follows: UGUCUAACCUCACCCUCUA, CAUCACACAGCUCCUCAAU, CGGAUUAUAUCUGUCCAAG, GAACAAAACUGCUCCAACA. Target sequences of the non-targeting control pool are as follows: UGGUUUACAUGUCGACUAA, UGGUUUACAUGUUGUGUGA, UGGUUUACAUGUUUUCUGA, UGGUUUACAUGUUUUCCUA. Cells were collected for western blot after 48 h. Western blot was performed three times and was quantified using ImageJ software. Statistical data were generated with Prism 9, and Student's *t*-test was performed to calculate the *P* value.

Lentivirus and stable cell line generation

For generating lentivirus, 750,000 HEK 293T cells were seeded in 6-well plates with DMEM supplemented with 10% FBS. After 24 h, the cells were transfected with the second-generation lentiviral packaging plasmids as well as the lentiviral plasmid of interest using Lipofectamine 3000. The virus-containing medium was collected 48 and 72 h after transfection, combined, clarified by centrifugation at 500*g* for 5 min, and then passed through a 45-μm PVDF filter. The purified virus was stored at 4 °C for short term use or aliquoted and frozen at −80 °C. For the generation of stable cell lines, HEK 293T cells were reverse transduced in 6-well plates in medium with 10 μg ml^{-1} polybrene using purified virus such that <30% of the cells are transduced. Twenty-four hours after transduction, the virus-containing medium was removed, and fresh medium was added. After another 24 h, the cells are collected, and transduction efficiency was confirmed via flow cytometry. Transduced cells are then selected with puromycin at 2 μg ml^{-1} for 48 h or via flow cytometry to generate a stable cell line for downstream analysis.

Generation of knockout cell lines

HEK 293T cells (7.5×10^5) were seeded in 6-well plates and transfected the next day with 4 μg of the lentiCRISPR v2 plasmid (Addgene #52961) containing a single guide RNA sequence specific to the targeted gene. After 24 h, cells were passaged into medium containing 2 μg ml^{-1} puromycin. After two days of puromycin selection, cells were collected, and single cells were sorted into 96-well plates. Individual clones were allowed to grow for 1–4 weeks and then passaged into 6-well plates. Clones were then screened for frameshift mutations in both alleles in the target gene using sanger sequencing and the ICE CRISPR analysis tool. Full knockout of the target genes was then verified using western blotting. Additionally, for *BAG6*-KO cells, the target locus was PCR amplified and cloned into plasmids. Sanger sequencing of 10 clones confirmed 2 frameshifting alleles, one with a 5-nt deletion, and the other with a 11-nt deletion.

Competitive growth assay

Wild-type HEK 293T and *BAG6*-KO (or *RNF126*-KO) cells were seeded at 2 million cells each into 10-cm plates with complete growth medium. After 72 h, cells were collected from both plates, passed through a 35-μm mesh cell strainer and quantified on a Countess II automated cell counter. The wild-type and knockout cells were then mixed in a 1:1 ratio and plated into three 10-cm plates. The cell mixtures were then cultured for an additional 15 days with genomic DNA collected about every three days. The guide RNA target region was amplified from the genomic DNA from all samples using Q5 High-Fidelity Master Mix and subsequently purified using a NucleoSpin Gel and PCR Clean-up kit

(Macherey-Nagel). The purified samples, including those from wild-type-only or knockout-only cells, were sent for Sanger sequencing. The proportion of wild-type and *BAG6*-KO cells in each sample was decomposed using a custom script adapted from TIDE[51]. The ratio of knockout to wild-type cells at each time point were then computed and plotted.

Flow cytometry analysis

Cells were collected and resuspended in 1–4 ml of fresh medium and passed through a 35-µm mesh cell strainer immediately prior to flow cytometry. Flow cytometry was performed on either a Bio-Rad ZE5 or NovoCyte Quanteon analyser. Gating of samples and export of data for downstream analysis was done using the FCS Express software.

RT–qPCR

SMAD4 mRNA expression in *SMAD4*-mutant and *BAG6*-KO cells. Stable cells were collected for RNA extraction, and quantitative PCR with reverse transcription (RT–qPCR) was performed to measure relative mRNA expression. Statistical data was generated with Prism 9, and Student's *t*-test or one-way ANOVA test was performed to calculate the *P* value. *SMAD4* mRNA expression in *RNF126*-knockdown cells. HEK 293T cells were seeded in 6-well plate with 2.5×10^5 cells per well, and transfected was performed next day. Twenty-five picomoles siControl (Horizon Discovery, D-001810-10-05) and 25 pmol siRNF126 (Horizon Discovery, L-007015-00-0005) were transfected with lipofectamine RNAiMAX, after 48 h, cells were collected for RNA extraction. RT–qPCR was performed to measure mRNA relative expression. Statistic data were generated with Prism 9, One-way ANOVA was performed to calculate the *P* value.

Generation of the Pep30 and Pep 13 reporter library

For the Pep30 library, a pool of 12,000 oligonucleotides were synthesized by Twist Bioscience, each containing a 90-nt variable sequence flanked by a 15-nt constant sequence on each side. The left constant sequence TACTGCGGCCGCTAC carries a NotI site, whereas the right constant sequence TGACTAGCTGACCTG contains stop codons (underlined) in all three reading frames, followed by a SbfI site (extended into the vector backbone) for cloning. The variable sequences were picked from a set of randomly selected lncRNAs[52], as well as the following regions in coding mRNAs (RefSeq): the 5′ end of internal coding exons (not the entire CDS), introns, 3′ UTRs, 5′ UTR ORFs, and the 3′ end of the last coding exon. Regions annotated to multiple classes or overlapping with each other on either strand were discarded. For introns and 3′ UTRs, the first 90 nt was used. For lncRNAs and 5′ UTRs, the first AUG was identified, and the next 90 nt were used. For C termini of CDS, the last 90 nt of the ORF (excluding the stop codon) were used. For internal CDS, the first 90 nt of individual internal coding exons were used, with about one third being in-frame with the eGFP ORF. The oligonucleotide pool was PCR amplified and then cloned into pJA291 using the NotI and SbfI sites and primers listed in Supplementary Table 4. The Pep13 library was cloned into pJA291 using the NEB Q5 Site-Directed Mutagenesis Kit (E0554) and two oligonucleotides listed in Supplementary Table 4. The forward oligonucleotide contains 39 random bases (IDT standard mixed base N).

Massively parallel reporter assays in HEK 293T cells

The Pep30 and Pep13 libraries were used to generate stable cell libraries of HEK 293T using lentiviral transduction such that each cell was integrated with at most one virus. Cells were then sorted into two bins: eGFP-high (top 30%, about 15 million cells) or eGFP-low (bottom 20%, about 10 million). Genomic DNA was isolated using QIAamp DNA Mini Kit from QIAGEN. The variable regions of the reporter were then PCR amplified using Phusion HF DNA polymerase (24 cycles). Gel-purified PCR products were sequenced using Illumina HiSeq 2000. Reads for each reporter sequence were counted directly from fastq files using the command "zcat $sample.fastq.gz | awk 'NR % 4 == 2' | sort | bedtools groupby -g 1 -c 1 -o count > $sample.counts.txt". The expression of each reporter sequence was calculated as the $\log_2$ read count ratio in eGFP-high bin relative to eGFP-low bin. The script used to generate Fig. 2 can be found in the Github depository.

Nucleotide level analysis

Pep30 library sequence diversity. Pairwise hamming distance (number of nucleotide difference) between any two sequences in the library was calculated and for each sequence, we then identified the shortest distance to any other sequence in the library. As a comparison, the same analysis was performed in a shuffled Pep30 library where each Pep30 sequence was shuffled while preserving mononucleotide frequency. Pep30 library 3-nt periodicity of U bias: for reporter sequences with more than 100 reads (high-GFP and low-GFP combined, 10,434 out of 12,000 sequences), an enrichment score in the low-GFP bin was calculated as the $\log_2$ ratio of read counts between the low-GFP bin and the high-GFP bin. kpLogo was then used to perform Wilcoxon rank-sum tests evaluating whether the presence of a particular nucleotide at each position is associated with a higher enrichment score. A logo plot was generated using Logomaker[53] in which the height of each nucleotide at each position was scaled by −log10(*P* value). Pep13 library 3-nt periodicity of U bias: we obtained 21,020,499 reads from 2,353,836 unique random 39-nt sequences in GFP-high cells, and 31,388,971 reads from 3,178,572 unique sequences in GFP-low cells. Sequences were translated in silico to determine peptide length and then grouped by peptide length (*L*). Each group contains more than 400,000 reads. For each peptide length group (*L* from 0 to 13), the fraction of A, C, G and U nucleotides at each position was calculated (unique sequences weighted by read counts) for GFP-high and GFP-low samples separately. The $\log_2$ ratio of nucleotide frequency was then used to generate sequence logo plots using Logomaker.

Massively parallel reporter assays comparing wild-type and *BAG6*-KO HEK 293T cells

HEK 293T as well as a clonal *BAG6*-KO cell line were reverse transduced with the Pep30 library such that less than 30% of cells were transduced (thus are most probably a single integration per cell). The virus-containing medium was removed after 24 h and fresh medium with 10% FBS and 1% PenStrep was added to the plates. After another 24 h, transduced cells were purified based on their expression of mCherry. The transduced populations were returned to culture and allowed to grow out for an additional 6 days, with passaging as necessary to maintain confluence below 80%. After 6 days, both populations were sorted into 4 bins based on the ratio of eGFP/mCherry expression (high, mid–high, mid–low, and low) using a FACSAria cell sorter. The same mCherry/eGFP ratio gates were used for both wild-type and *BAG6*-KO cells. Sorted cells were spun down at 500*g* for 5 min, washed once with 1,000 µl PBS, spun down again, then frozen at −20 °C as a cell pellet. Genomic DNA was subsequently isolated from the cell populations using a Machery Nagel Nucleospin Tissue kit and genomic DNA was eluted in 50 µl of elution buffer. Libraries were then amplified using PCR with custom Illumina adapters, using Q5 high-fidelity PCR mix with 1,000 ng input gDNA per sample. Libraries were amplified for a total of 24–27 cycles. After amplification, libraries were cleaned up up using SPRISelect beads at a ratio of 0.7×. Purified library size was confirmed via gel and libraries were quantified using the KAPA qPCR Illumina library quantification kit. Libraries were subsequently pooled in a ratio based on the number of total cells collected from each sample. The pooled library was sequenced on a NextSeq 550 with 2.5% PhiX spike in, using the 75-cycle high-output kit with 80 cycles in read 1 and 8 cycles in index read 1. Reads were aligned to a custom index for the Pep30 library generated with the command bowtie-build in bowtie version 1.2.3 and the option -v 3 --best (best alignment with up to 3 mismatches). The counts of each Pep30 sequence were extracted

from the alignment with the bash command cut -f 3 | sort | uniq -c. For each sequence, a normalized expression value was calculated using its counts in all four bins. In brief, we first calculated the slope of read count changes from low, mid–low, mid–high to high eGFP/mCherry bins. Sequences with more reads in lower ratio bins will have a more negative slope, whereas sequences with more reads in higher ratio bins will have a more positive slope. We then used an inverse logit transformation to convert the slope to a normalized 'expression' value between 0 and 1. Only sequences encoding a full-length 30-aa peptide and have at least 3,000 total reads (combining all 4 bins) were used in the analysis.

Genome-wide CRISPR screen

The Human Activity-Optimized CRISPR Knockout Library (3 sub-libraries in lentiCRISPRv1) was obtained from Addgene (#1000000100) and prepared according to the standard protocol. Library lentivirus was produced using Mirus LT1 transfection reagent and second-generation packaging plasmids. In total, 9.2×10^7 HEK 293T cells carrying the stable *AMD1*-eGFP reporter were reverse transduced with the CRISPR library with 8 μg ml^{-1} polybrene. Medium was changed 24 h after transduction. Selection with 2 μg ml^{-1} puromycin was initiated 48 h after transduction. After 48 h of puromycin selection, cells were collected and sorted, sorted cell populations were frozen at −80 °C. Libraries were prepared for Illumina sequencing from the sorted cell populations as described in ref. 54. Libraries were amplified for a total of 28 PCR cycles, purified using the Zymo DNA Clean & Concentrator-5 kit, and the correct-sized band was subsequently purified by gel extraction. Fragment sizes of the libraries were confirmed by bioanalyzer and concentrations were determined using the KAPA qPCR library quantification kit. The pooled library was then sequenced on a NextSeq 550 with 86 cycles in Read 1 and 6 cycles in Index Read 1. MAGeCK[55] was used to analyse the CRISPR screen result.

Co-immunoprecipitation

HEK 293T cells were seeded in 10-cm plates with 3×10^6 cells per plate. Reporters were transfected into the cells 24 h after seeding using Lipofectamine 3000. Forty-eight hours after transfection, cells were treated with DMSO (vehicle) or 0.1 μM bortezomib. After 24 h of drug treatment, cells were collected, washed twice in cold PBS, and resuspended in lysis buffer (0.025 M Tris pH 7.4, 0.15 M NaCl, 0.001 M EDTA, 1% NP-40 alternative, 5% glycerol). Lysates were incubated at 4 °C with rotation for 30 min, centrifuged at 12,000*g* at 4 °C for 20 min, and the supernatant was collected. The pulldowns were performed using Novex DYNAL Dynabeads, Protein G-conjugated with a primary antibody according to the manufacturers protocol. Following co-immunoprecipitation, western blots were performed as described below.

Western blotting

Cells were cultured and transfected where applicable as described above. Cells were collected on ice and washed with cold PBS and subsequently lysed in RIPA buffer supplemented with a 1× protease inhibitor cocktail for 30 min at 4 °C on a rotator. Lysates were then cleared by centrifugation at 16,000*g* and 4 °C for 20 min. Protein concentrations were determined using a BCA assay and samples were then prepared using LDS sample buffer supplemented with sample reducing agent and heated to 70 °C for 10 min. Samples were then run on an SDS-PAGE gel and transferred to an activated PVDF membrane for 90 min at 30 volts or overnight at 10 volts. Membranes were blocked with 5% BSA in PBS-T for 1 h at room temperature or overnight at 4 °C. Membranes were then cut and incubated with the appropriate primary antibody in blocking buffer supplemented with 0.02% sodium azide for 1 h at room temperature or overnight at 4 °C. Secondary antibodies were added at a 1:10,000 dilution and incubated for 1 h at room temperature. Immobilon ECL Ultra Western HRP Substrate was then added to the membranes and blots were visualized using an Amersham Imager 600.

In-gel proteasome activity

Cells were collected in a buffer containing 50 mM tris-HCl (pH 7.4), 5 mM $MgCl_2$, 5 mM ATP, 1 mM dithiothreitol, 1 mM EDTA, 10 mM NAF (Sodium fluoride), 25 mM β-glycerolphosphate, phosphatase inhibitors, and 10% glycerol, which preserved 26S proteasome assembly. The samples (3 biological replicates per condition: control, BAG6 knockout, and TRC35 knockout) were homogenized and centrifuged at 20,000*g* for 25 min at 4 °C. The supernatant was collected and normalized for protein concentration determined by Bradford assay. Samples (40 μg protein per well) were loaded on 4% non-denaturing gels and run for 190 min at 160V in buffer containing 180 mM boric acid, 180 mM Trizma base, 5 mM $MgCl_2$, 1 mM ATP, and 1 mM dithiothreitol. The gels were incubated for approximately 10 min at 37 °C in buffer containing 50 mM Tris-HCl, 5 mM $MgCl_2$, 5 mM ATP, 1 mM dithiothreitol, 10% glycerol, and 125 μM of the fluorogenic proteasome substrate Suc-LLVY-amc (Enzo Life Sciences). 26S proteasome activity bands were detected by transilluminator with 365-nm light and photographed by iPhone 10S camera. The same samples used for in-gel proteasome activity were run in parallel for western blotting to determine levels of the 26S proteasome. Samples (60 μg protein per well) were loaded on 4% non-denaturing gels and run under the same conditions as gels for activity. Gels were transferred to 0.2-μm nitrocellulose membranes, blocked in 5% milk, and incubated with primary mouse anti-proteasome 20S α1, 2, 3, 5, 6 and 7 subunits monoclonal antibody (1:2,000, Enzo Life Sciences) in SuperBlock Buffer (ThermoFisher) overnight at 4 °C and secondary anti-mouse antibody (1:3,000) in 5% milk for two hours at room temperature. Membranes were developed with enhanced chemiluminescent reagent Immobilon Western HRP substrate and Luminol reagent (Millipore) using a Fujifilm LAS3000 imaging system. Samples (10.5 μg protein/well for actin or 22.5 μg protein per well for ubiquitinated proteins) were also run on NuPAGE 4–12% Bis-Tris gels (Invitrogen) under denaturing conditions and immunoblotted for actin or ubiquitinated proteins using the same procedure above using primary anti-mouse actin antibody (1:7000) or rabbit anti-K48 linkage polyubiquitin antibody (1:2,000, Cell Signaling Technologies) and secondary anti-mouse or anti-rabbit antibody (1:3,000). ImageJ (http://rsb.info.nih.gov/ij) was used to quantify the signal from 26S proteasome activity (in-gel proteasome activity assay) and 26S proteasome levels (western blot). Relative activities and levels were calculated for each sample and averaged across the four technical replicates for each sample. These values were then normalized by actin levels for each condition. The results were used to compare proteasome level and activity of each of the knockouts relative to the control. Statistical analysis was performed with GraphPad Prism9 using one-way ANOVA to compare groups. Data are expressed as mean ± s.e.m. for the three biological replicates, with $P < 0.05$ considered significant.

Correlation between mitigation and physiochemical and structural properties of tail peptides

Secondary structures of each peptide were predicted using S4PRED[56], which outputs a vector indicating whether each residue is in an α-helix, β-sheet or coil. The number of residues in each of the secondary structure motif in a peptide is used to calculate the correlation with mitigation. Protein intrinsic disorder was calculated using the program IUPred3, specially for short disorder analysis without smoothing. The disorder score for each residue in a peptide is added together and the total disorder score is used to calculate correlation with mitigation. All other properties were calculated using the following functions in the R package Peptides[57]: Average_hydrophobicity: hydrophobicity using the Miyazawa scale[58] unless otherwise noted (Extended Data Fig. 2); hydrophobic moment: hmoment, amino acid composition (*.AA.count): aacomp, mass-to-charge ratio: mz, molecular weight: mw, net charge: charge, interaction potential: boman, instability index: instaIndex, and transmembrane potential: membpos.

Genome-scale hydrophobicity analysis

We systematically compared C-terminal hydrophobicity of proteins encoded by coding and noncoding sequences (Fig. 2f). The CDS of annotated proteins were downloaded from Ensembl (Homo_sapiens.GRCh38.cds.all.fa) and translated into proteins using BioPython. Only proteins with more than 200-aa were used for downstream analysis. The cDNA sequences for protein-coding and long noncoding RNA transcripts (lncRNA) were obtained from GENCODE v37. From the coding transcripts the 5′ UTR and 3′ UTR sequences were extracted. For both 5′ UTR and lncRNA, the longest ORF was translated into peptides. For 3′ UTR and introns, the first in-frame stop codon marks the end of the tail ORF and only those with at least 30 codons were used. Noncoding sequence encoded peptides were removed if found in the canonical proteome. For each group, the average hydrophobicity at each position relative to the last amino acid (the most C-terminal) was calculated using the hydrophobicity function in the R package Peptides[57]. To rule out that the depletion of hydrophobicity is due to the lack of protein domains (which are often hydrophobic), a subset of proteins depleted of annotated protein domains NCBI Conserved Domain Database[59] (CDD) in the last 100 aa were analysed.

Correlation between C-tail hydrophobicity and gene age

Gene age was inferred by a previous study[34]. In brief, human and mouse genes were assigned to branches of the vertebrate phylogenetic tree based on the presence and absence of orthologues in various species. The age of the genes in a branch is calculated as the middle point of each branch. The average hydrophobicity of the last 30 aa of all genes in a branch was calculated using the R package Peptide described above.

Reporting summary

Further information on research design is available in the Nature Portfolio Reporting Summary linked to this article.

Data availability

The sequencing data for the massively parallel reporter assay has been deposited in the Gene Expression Omnibus with the accession number GSE208661. Uncropped gel images are included in Supplementary Fig. 1. Gating strategies for flow cytometry assays are included in Supplementary Fig. 2.

Code availability

Scripts for data analysis are available at https://github.com/xuebingwu/noncoding-translation-code.

51. Brinkman, E. K., Chen, T., Amendola, M. & van Steensel, B. Easy quantitative assessment of genome editing by sequence trace decomposition. *Nucleic Acids Res.* **42**, e168 (2014).
52. Hezroni, H. et al. Principles of long noncoding RNA evolution derived from direct comparison of transcriptomes in 17 species. *Cell Rep.* **11**, 1110–1122 (2015).
53. Tareen, A. & Kinney, J. B. Logomaker: beautiful sequence logos in Python. *Bioinformatics* **36**, 2272–2274 (2020).
54. Joung, J. et al. Genome-scale CRISPR–Cas9 knockout and transcriptional activation screening. *Nat. Protoc.* **12**, 828–863 (2017).
55. Li, W. et al. MAGeCK enables robust identification of essential genes from genome-scale CRISPR/Cas9 knockout screens. *Genome Biol.* **15**, 554 (2014).
56. Moffat, L. & Jones, D. T. Increasing the accuracy of single sequence prediction methods using a deep semi-supervised learning framework. *Bioinformatics* **37**, 3744–3751 (2021).
57. Osorio, D., Rondon-Villarreal, P. & Torres, R. Peptides: a package for data mining of antimicrobial peptides. *R J.* **7**, 4–14 (2015).
58. Miyazawa, S. & Jernigan, R. L. Estimation of effective interresidue contact energies from protein crystal structures: quasi-chemical approximation. *Macromolecules* **18**, 534–552 (1985).
59. Lu, S. et al. CDD/SPARCLE: the conserved domain database in 2020. *Nucleic Acids Res.* **48**, D265–D268 (2020).

Acknowledgements The authors thank D. Bartel for supporting some of the early work on this project; C. Zhang, P. Sims, B. Honig and M. AlQuraishi for discussion; and S. Diederichs for sharing the *SMAD4* readthrough cells. X.W. is supported by NIH Director's New Innovator Award (1DP2GM140977), Pershing Square Sohn Prize for Cancer Research, Pew-Stewart Scholar for Cancer Research Award, and the Impetus Longevity Grants. N.M. is supported by the National Institute of Aging (NIA) grants R01AG064244 and RF1AG070075. This research was funded in part through the NIH/NCI Cancer Center Support Grant P30CA013696 and used the Genomics and High Throughput Screening Shared Resource and CCTI Flow Cytometry Core. The CCTI Flow Cytometry Core is supported in part by the Office of the Director, National Institutes of Health under awards S10RR027050 and S10OD020056. The content is solely the responsibility of the authors and does not necessarily represent the official views of the National Institutes of Health.

Author contributions J.S.K. and Z.C. performed the majority of experiments. P.S. performed BAG6 and RNF126 overexpression and *RNF126* knockdown. A.O.A. generated *AMD1*-deletion reporters, the *SMAD4* readthrough reporter, and assisted in validating the *BAG6*-KO cell line. A.T., M.R.M., P.S. and Y.G. cloned and analysed representative noncoding sequences in multiple reporters. P.S. and Y.G. performed the *XBP1* reporter assay. J.S.K. and M.R.M. performed SMAD4–BAG6 co-immunoprecipitation. J.E.L. and N.M. performed in-gel proteasome activity assays. Y.R. assisted in sequencing the replicate of Pep30 rescue in *BAG6*-KO cells. X.W. initiated and supervised the project. J.S.K. and X.W. drafted the manuscript with input from all authors.

Competing interests The authors declare no competing interests.

Additional information
Supplementary information The online version contains supplementary material available at https://doi.org/10.1038/s41586-023-05946-4.

Correspondence and requests for materials should be addressed to Xuebing Wu.

Peer review information *Nature* thanks Hiroyuki Kawahara, Tobias von der Haar and the other, anonymous, reviewer(s) for their contribution to the peer review of this work. Peer review reports are available.

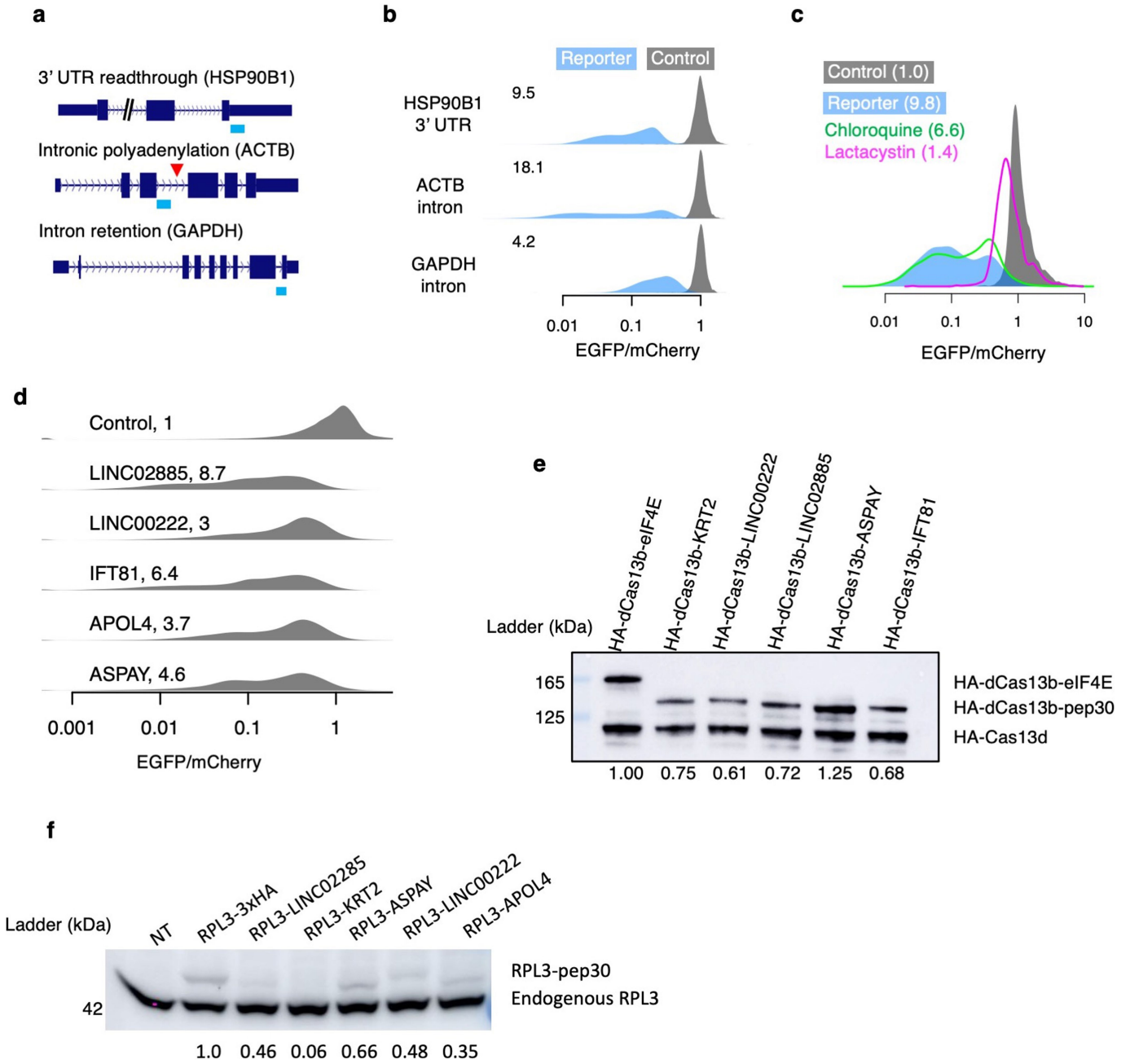

Extended Data Fig. 1 | Translation surveillance of representative noncoding sequences. a, Noncoding sequences in the *HSP90B1* 3' UTR, an *ACTB* intron, and a *GAPDH* intron were cloned into the bicistronic reporter system shown in Fig. 1b. **b**, Density plots for the distribution of EGFP/mCherry ratios as measured by flow cytometry 24 hours after reporter transfection. The median fold loss of EGFP/mCherry ratio relative to control is shown on the top left corner of each density plot. **c**, Density plot of the EGFP/mCherry ratio for cells transfected with either the control or the ACTB intron reporter, alone or with simultaneous treatment of either proteasome inhibitor (lactacystin) or lysosome inhibitor (chloroquine). The numbers indicate the median fold loss of EGFP/mCherry relative to control. **d**–**f**, six noncoding sequences from the Pep30 library (KRT2 intron, APOL4 intron, LINC00222, LINC02885, ASPAY 3' UTR, and IFT81 3' UTR) were selected and cloned into either the original mCherry-EGFP bicistronic reporter (**d**, cloning failed for KRT2), fused to the C-terminus of HA-tagged PspCas13b protein (**e**, cloning failed for APOL4), or fused to the C-terminus of RPL3 (**f**, cloning failed for IFT81). **d**, Same as **b** for indicated noncoding sequences. **e**, Equal amount of HA-dPspCas13b-pep30 reporter plasmids were co-transfected with a HA-RfxCas13d plasmid and the protein abundance was assayed by western blotting with an HA antibody. HA-dCas13b fused to human protein eIF4E was used as a control. The abundance of HA-dCas13b-pep30 was quantified by first normalizing to HA-Cas13d then to eIF4E fusion. **f**, Equal amount of RPL3 reporter plasmids were transfected into HEK293T cells and western blots were performed using an RPL3 antibody, which detects both endogenous RPL3 (lower bands) and the RPL3 reporter protein (upper bands). NT: no transfection control. The level of the reporter protein was first normalized to endogenous RPL3 and then to the RPL3-3xHA sample. N = 4 biological replicates.

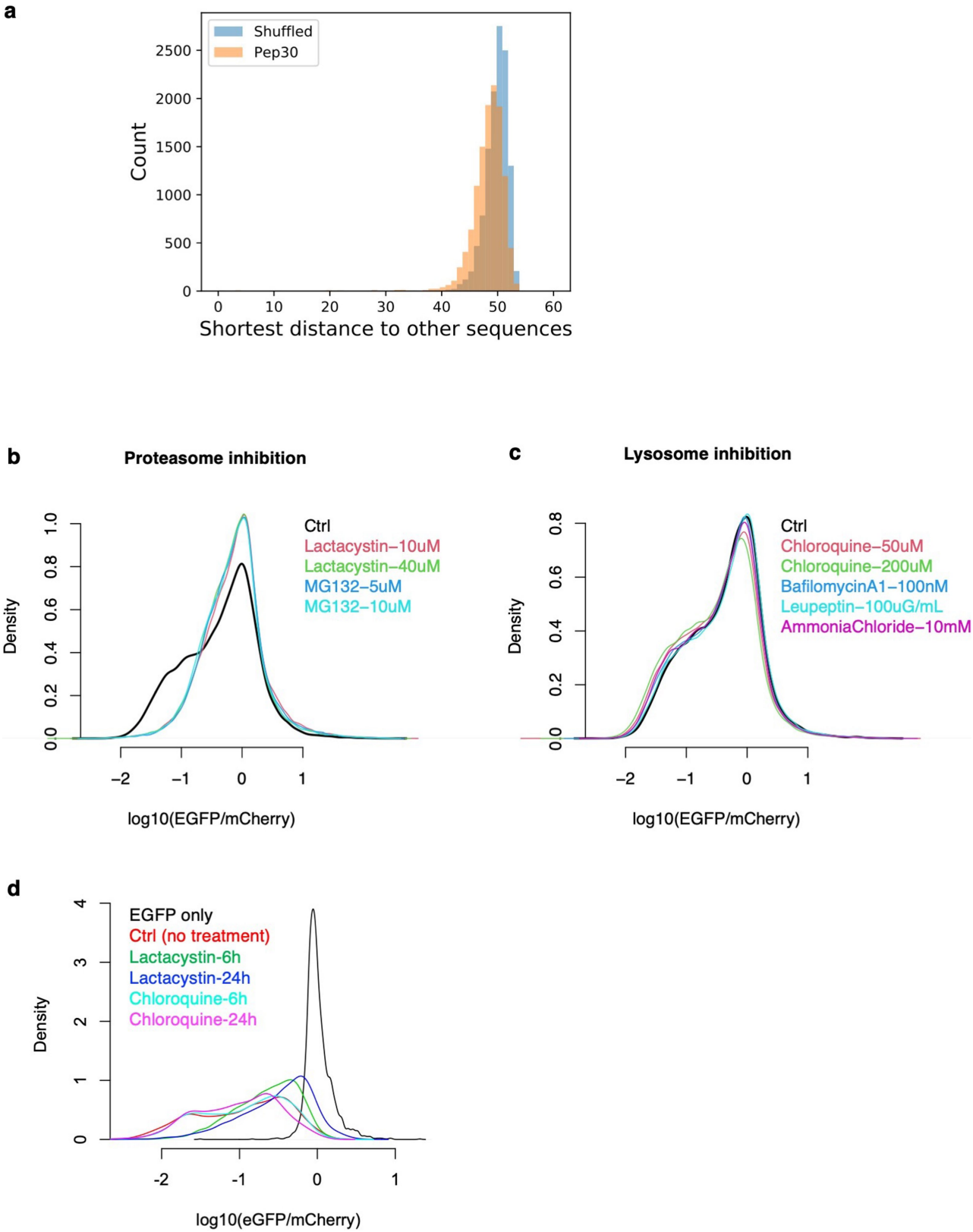

Extended Data Fig. 2 | Characterization of the Pep30 library. a, Sequence diversity in the Pep30 library. The pairwise hamming distance (number of nucleotides that are different) between any two sequences (of 90-nt) in the library was calculated. Subsequently for each sequence, we identify the shortest distance to any other sequence in the library. The result showed that the vast majority (98%) of Pep30 sequences are at least 40 nt (out of 90 nt) different from other sequences in the library, with a median distance of 48. This is very close the distribution when the Pep30 library sequences are shuffled (median: 50). The result indicated that our Pep30 library is nearly as diverse as one can get from entirely unrelated sequences. **b**–**d**, Effect of proteasome inhibition or lysosome inhibition on the Pep30 library. **b**, Pep30 cells were treated with proteasome inhibitors for 8 h and then analyzed with flow cytometry. Ctrl: Pep30 cells without treatment. **c**, Same as (**b**) for multiple lysosome inhibitors. **d**, longer (24 h vs. 6 h) proteasome inhibition but not lysosome inhibition resulted in more rescue.

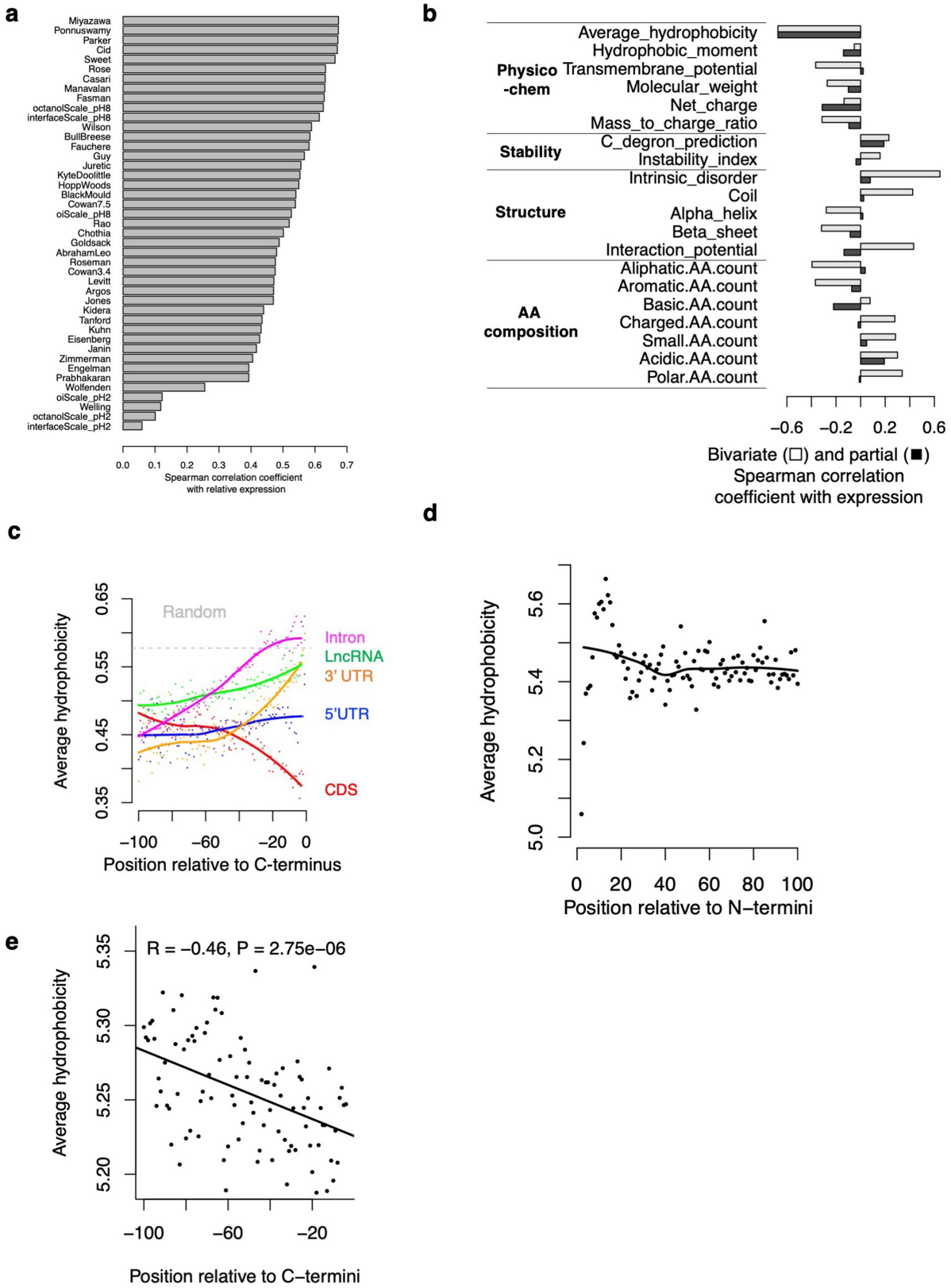

Extended Data Fig. 3 | Hydrophobicity analyses in the Pep30 library and the human genome. a, The correlation coefficient between Pep30 reporter expression and average hydrophobicity calculated using various scales. **b**, Spearman correlation coefficient (light bar) between various properties of the Pep30 sequences and reporter expression. Dark bar: partial correlation conditioned on average hydrophobicity. **c**. Same as Fig. 2f with a different hydrophobicity scale (Ponnuswamy instead of Miyazawa). **d**, Average hydrophobicity for the first 100 aa (N-termini) of annotated proteins (N = 38,933). **e**, Average hydrophobicity of the C-termini of annotated proteins without any annotated protein domains in the last 100aa (N = 8,586). Shown are the Spearman correlation coefficient R and the P value of a two-sided Spearman's correlation test. No adjustments were made for multiple comparisons.

a

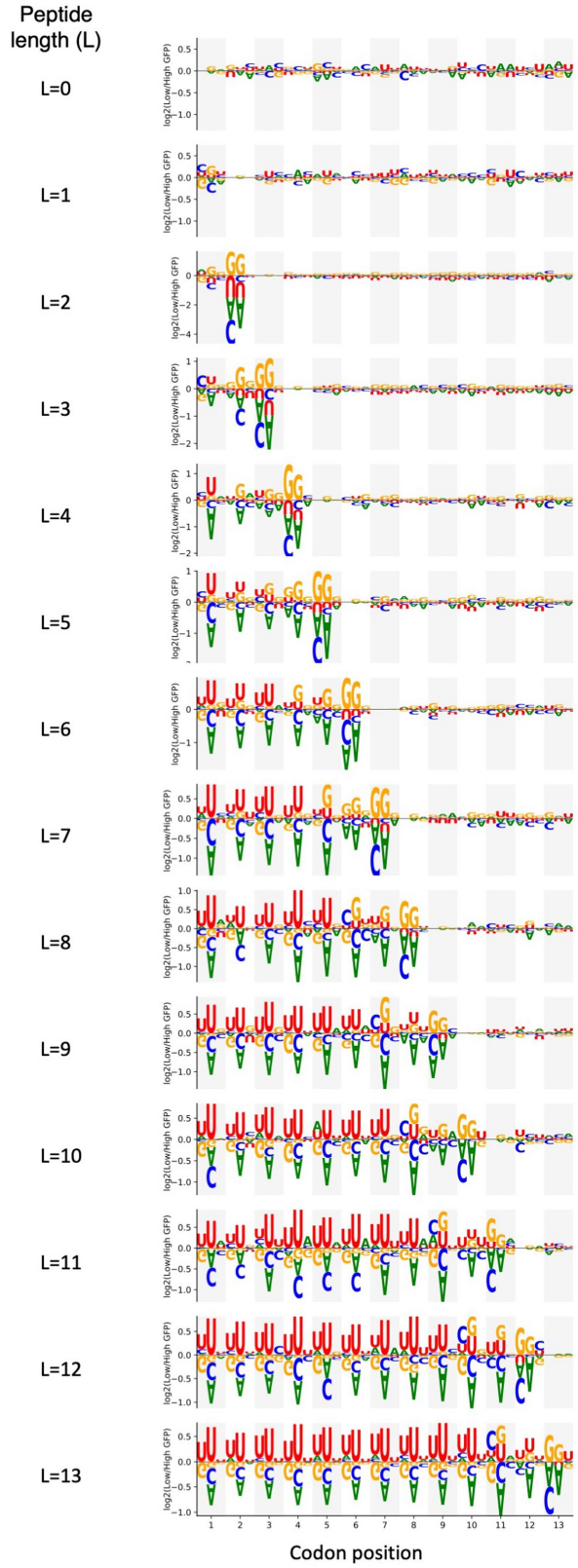

b

F	UUU	9.03
F	UUC	9.03
M	AUG	8.95
I	AUU	8.83
I	AUC	8.83
I	AUA	8.83
L	UUA	8.47
L	UUG	8.47
L	CUU	8.47
L	CUC	8.47
L	CUA	8.47
L	CUG	8.47
C	UGU	7.93
C	UGC	7.93
W	UGG	7.66
V	GUU	7.63
V	GUC	7.63
V	GUA	7.63
V	GUG	7.63
Y	UAU	5.89
Y	UAC	5.89
A	GCU	5.33
A	GCC	5.33
A	GCA	5.33
A	GCG	5.33
H	CAU	5.1
H	CAC	5.1
U	ACU	4.49
U	ACC	4.49
U	ACA	4.49
U	ACG	4.49
G	GGU	4.48
G	GGC	4.48
G	GGA	4.48
G	GGG	4.48
R	CGU	4.18
R	CGC	4.18
R	CGA	4.18
R	CGG	4.18
R	AGA	4.18
R	AGG	4.18
S	UCU	4.09
S	UCC	4.09
S	UCA	4.09
S	UCG	4.09
S	AGU	4.09
S	AGC	4.09
P	CCU	3.87
P	CCC	3.87
P	CCA	3.87
P	CCG	3.87
Q	CAA	3.87
Q	CAG	3.87
N	AAU	3.71
N	AAC	3.71
E	GAA	3.65
E	GAG	3.65
D	GAU	3.59
D	GAC	3.59
K	AAA	2.95
K	AAG	2.95

c

	U/T	A	C	G
Intron	31.0%	28.4%	19.9%	20.7%
3' UTR	28.3%	26.8%	22.5%	22.4%
Genome	26.6%	28.0%	22.7%	22.7%
LncRNA	26.6%	28.0%	22.7%	22.7%
Coding	21.7%	25.2%	26.5%	26.5%
5' UTR	21.7%	22.6%	27.7%	28.0%

Extended Data Fig. 4 | Bias in the genetic code drives hydrophobicity. a, Same as Fig. 3b (right) for all peptide lengths. **b**, Codons ranked by the hydrophobicity of the corresponding amino acids. **c**, Nucleotide composition in different types of regions in the human genome.

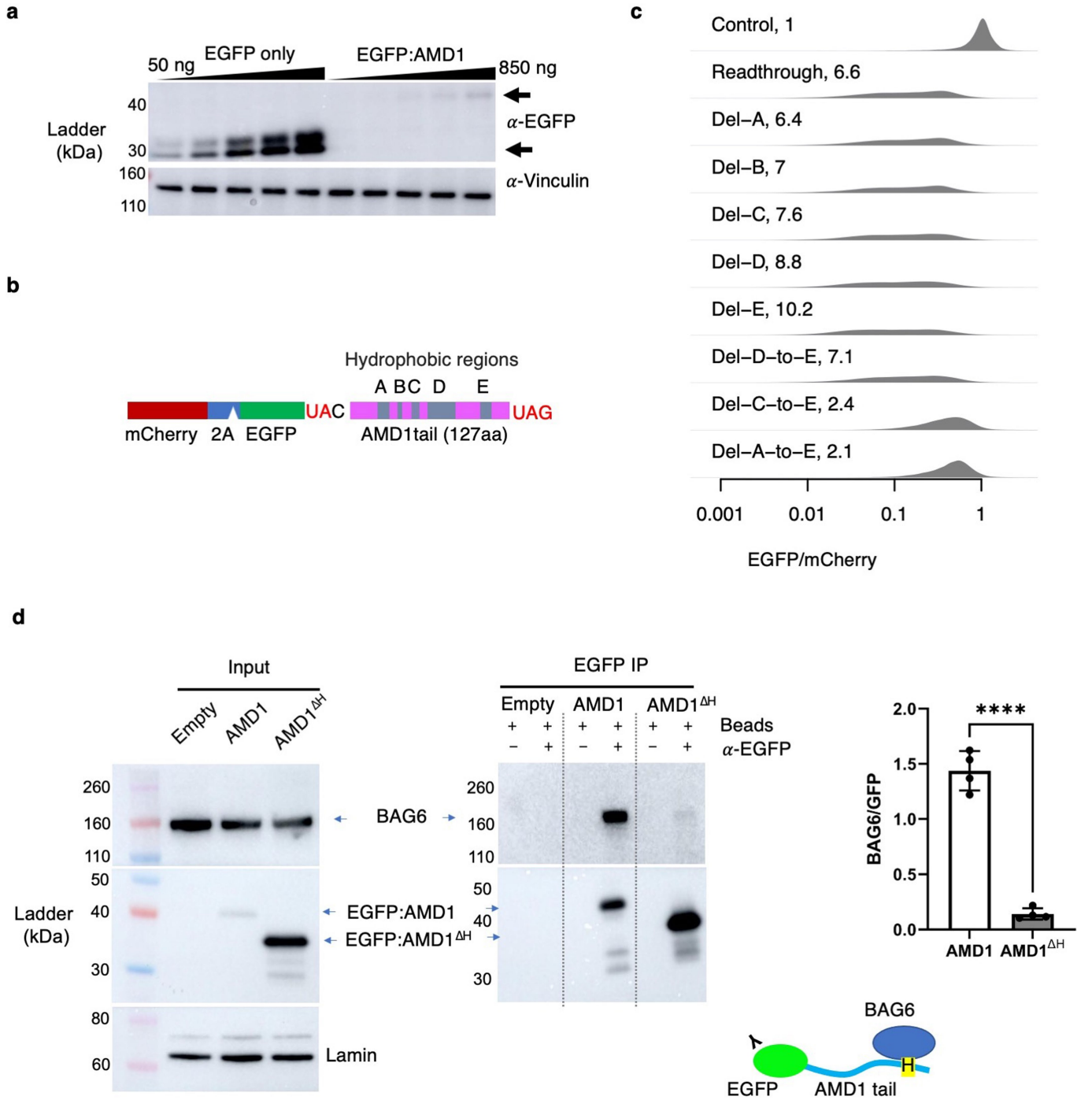

Extended Data Fig. 5 | AMD1 3′ UTR translation mitigation. a, Western blot confirming the loss of the EGFP-AMD1 tail fusion protein. HEK293T cells were transfected with varying amount of the AMD1 3′ UTR readthrough reporter plasmid, from 50 ng to 850 ng. (N = 2 biologically independent samples). **b**, The AMD1 3′ UTR translation reporter with the hydrophobic region in the AMD1 tail highlighted (A-E). **c**, Impact of deleting individual hydrophobic regions or larger regions on the EGFP/mCherry ratio. The number in each plot is the median decrease of the EGFP/mCherry ratio relative to controls. **d**, BAG6 co-immunoprecipitates with EGFP:AMD1 fusion protein but not a mutated fusion protein with the functional hydrophobic region C-to-E deleted ($AMD1^{\Delta H}$). N = 4 biologically independent samples over 2 independent experiments for the quantification. Data are presented as mean values +/− s.d. P values calculated using two-sided Student′ t-test. No adjustments were made for multiple comparisons. ****: P < 0.0001.

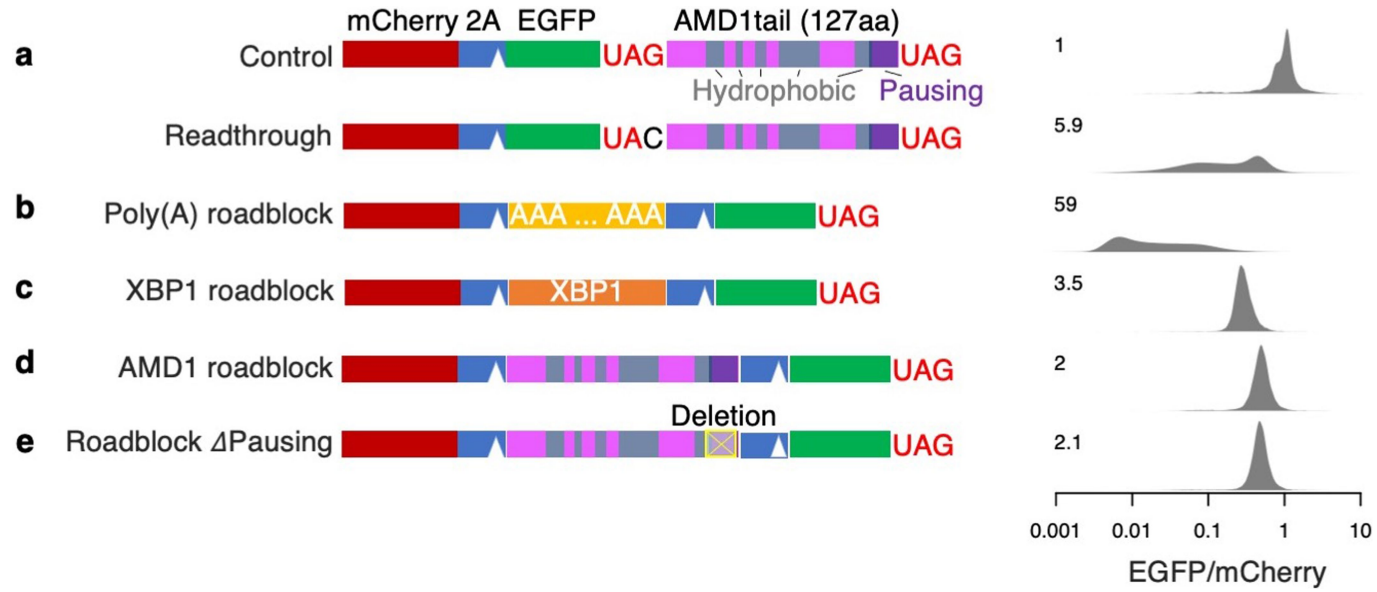

Extended Data Fig. 6 | Ribosome roadblock effect: comparing the AMD1 tail sequence, poly(A) and the XBP1 stalling sequence. a–**e**, Reporter constructs shown on the left were transfected into HEK293T cells. The EGFP/mCherry ratio was quantified in individual cells using flow cytometry with distributions shown on the right on a log-10 scale. The number in each plot is the median fold-decrease of the EGFP/mCherry ratio. Note that AMD1 sequence causes less decrease in EGFP compared to both XBP1 and poly(A) sequences, and even this weak effect is independent of the putative pausing sequence in AMD1.

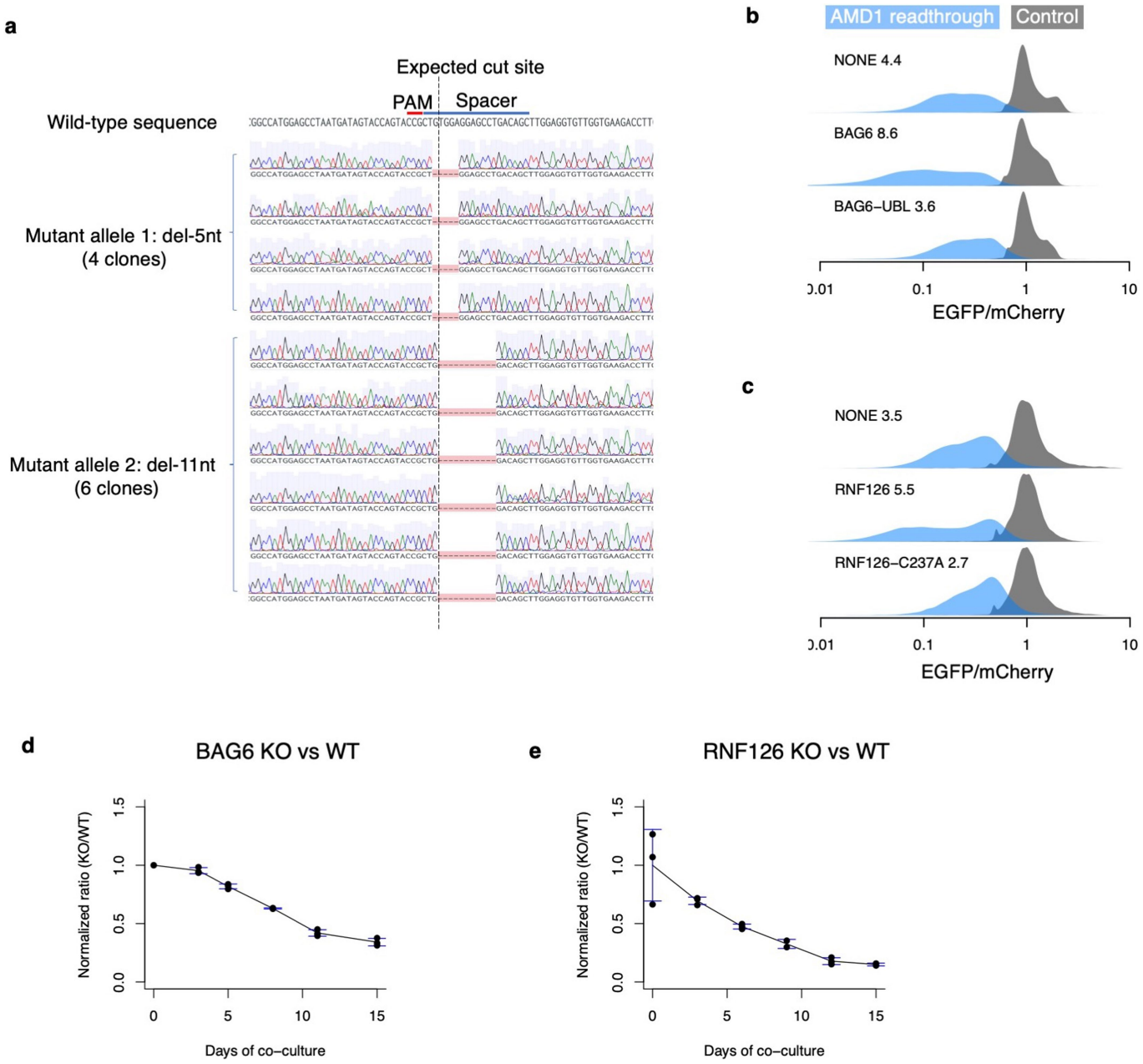

Extended Data Fig. 7 | Characterization of the BAG6 KO cells and RNF126 KO cells. a, Genotyping the BAG6 clonal knockout cell line. Sanger sequencing of 10 clones of PCR-amplified genomic DNA confirmed that the BAG6 KO cells contain a frameshift mutation in both alleles, one with a 5-nt deletion and the other with an 11-nt deletion around the expected Cas9 cut site. **b**, Re-expressing wild type BAG6 but not an inactive mutant missing the UBL domain for recruiting RNF126 (BAG6-UBL) partially reverses BAG6 KO phenotype as measured by the destabilization of AMD1 readthrough product. **c**, Same as **b** but comparing wild type RNF126 and an inactive mutant with a C237A mutation in the active site. **d**-**e**, Growth defect of BAG6 KO cells (**d**) and RNF126 KO cells (N = 3 biologically independent samples) (**e**) revealed by competitive growth assays. KO cells and WT cells were mixed and co-cultured for 15 days and the relative cell numbers (KO/WT) at each time point was determined by decomposition of sanger sequencing traces as described in Methods. N = 1 for day 0 of BAG6 and N = 3 biologically independent samples for all other time points. Data are presented as mean values +/− s.d.

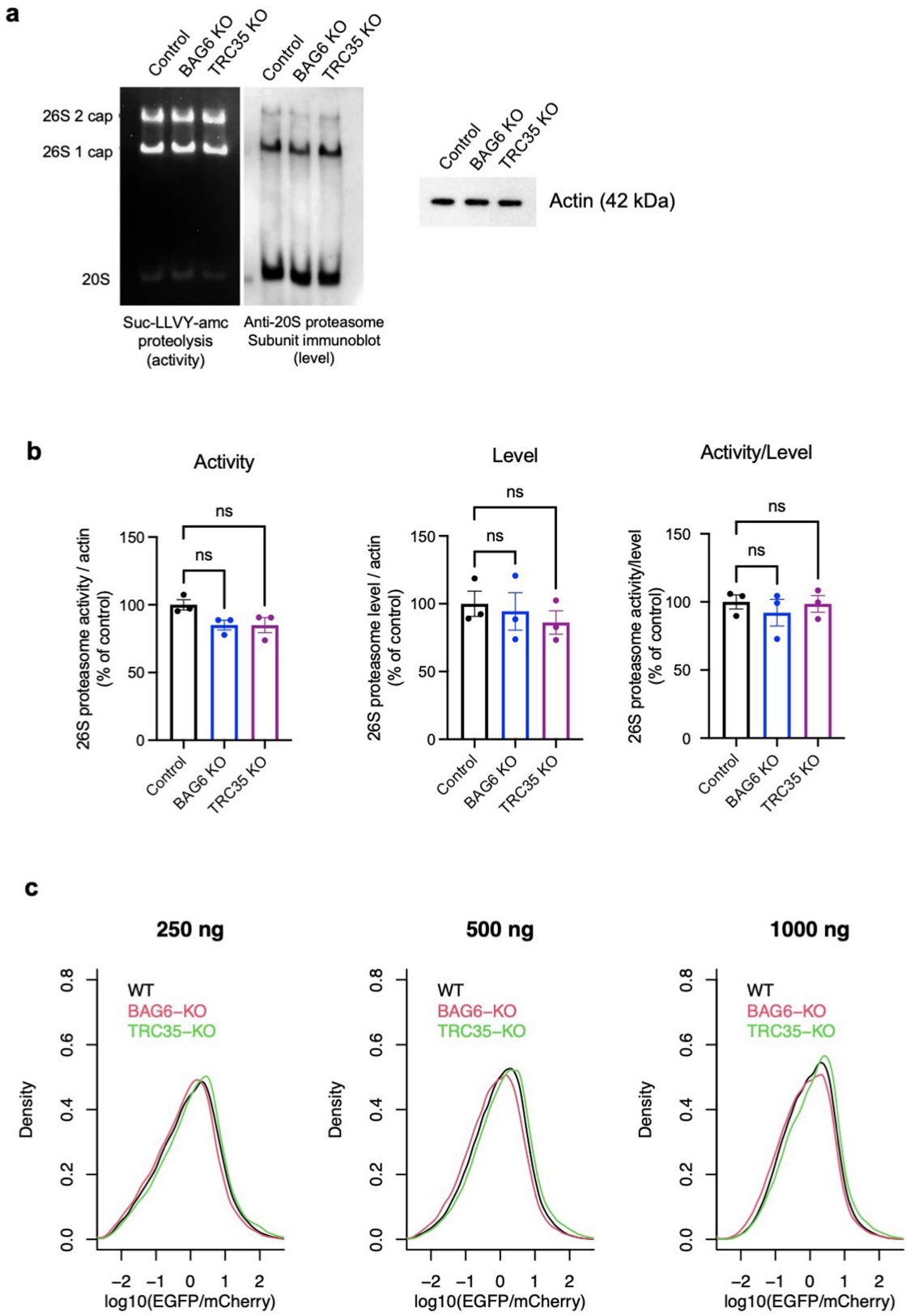

Extended Data Fig. 8 | See next page for caption.

Extended Data Fig. 8 | BAG6 or TRC35 knockout does not affect proteasome activity or level. a, Representative result from in-gel proteasome activity assay showing proteasome hydrolysis activity (left) and representative immunoblot probing for a subunits levels of the 26S 1- and 2-cap proteasome and 20S proteasome (middle). Cell lysates were run on 4% non-denaturing (native) gels and incubated with fluorogenic Suc-LLVY-amc proteasome substrate to determine relative activities or immunoblotted to determine relative levels. Samples (10.5 µg protein/well) were run separately under denaturing conditions for immunoblot probing for actin as a sample processing control (right). **b**, The level of 26S 1- and 2-cap proteasome detected by immunoblotting normalized to actin in the same sample (left), densitometric quantification of 26S 1- and 2-cap proteasome in-gel activity normalized by actin in the same sample (middle), and the activity/level ratio (right). Data are expressed mean ± SEM for three biological replicates, where each value represents the activity/level ratio calculated by averaging four technical replicates of activity and level values. One-way ANOVA was used for statistical analysis, with $P < 0.05$ considered significant. **c**, Similar result with in vivo proteasome activity reporter assays. The proteasome activity reporter Ub^{G76V}-EGFP was co-transfected with mCherry (1:1) into cells and the EGFP/mCherry ratio measured by flow cytometry was used as an indicator of proteasome activity in cells. The distribution the EGFP/mCherry ratio in WT, BAG6 KO, and TRC35 KO cells at 250 ng, 500 ng, and 1000 ng total plasmid were shown.

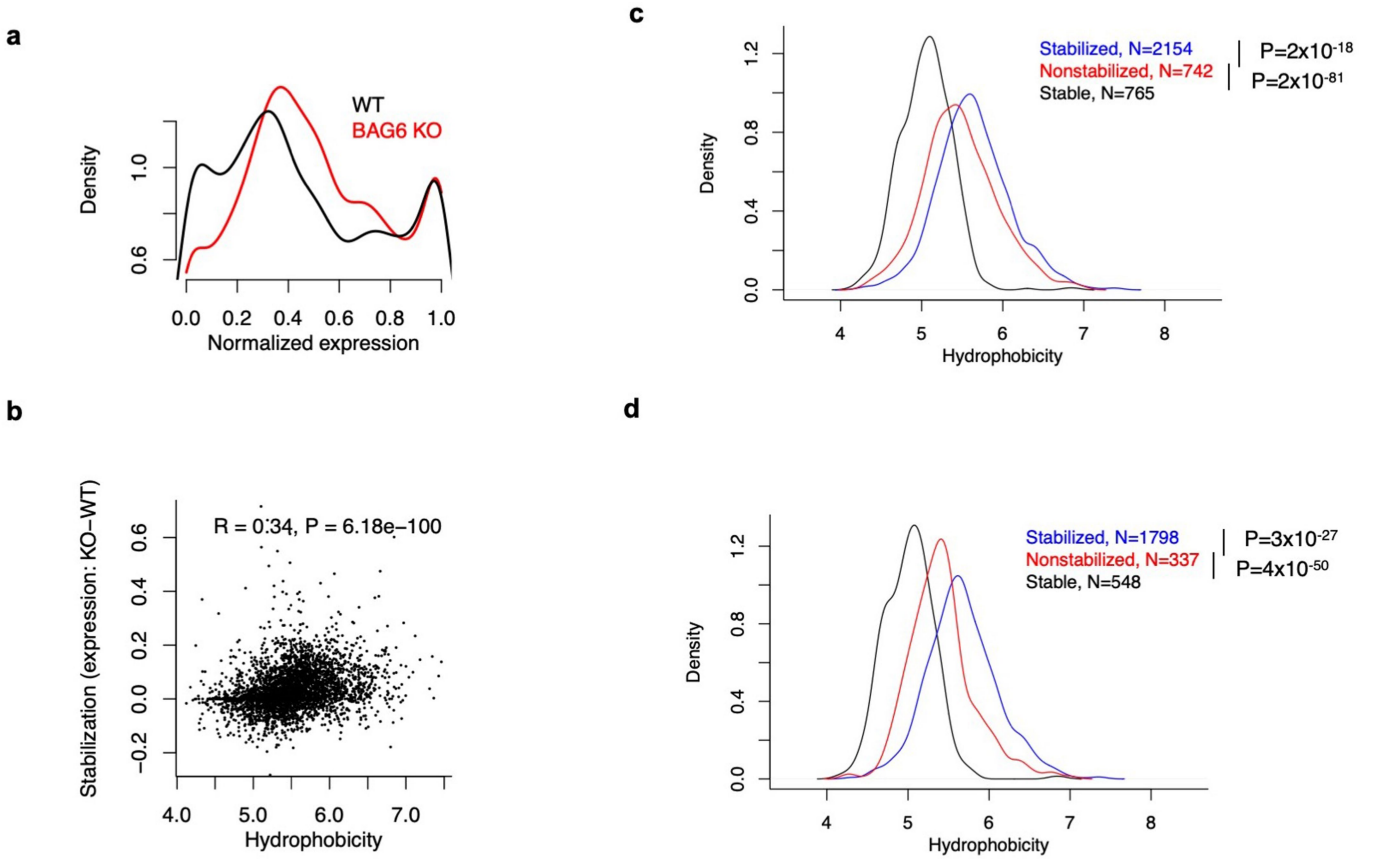

Extended Data Fig. 9 | Replicating the Pep30 reporter assay in BAG6 KO cells. The sequencing-based assay shown in Fig. 5f–h was repeated starting from cell sorting. **a**, Same as Fig. 5g. **b**, Same as Fig. 5h. **c**, full-length Pep30 reporter sequences with a minimum of 3000 reads (all four bins combined) were divided into three groups: those that are stable in wild-type cells (normalized expression >0.8), those that are unstable in wild type cells but are stabilized (increased expression) in BAG6 KO cells, and those that are unstable in wild type cells and are not stabilized in BAG6 KO cells. Shown are the density plot of the hydrophobicity of sequences in each group. **d**, same as **c** for the replicate shown in Fig. 5. P values were calculated using two-sided Mann-Whitney U test. No adjustments were made for multiple comparisons.

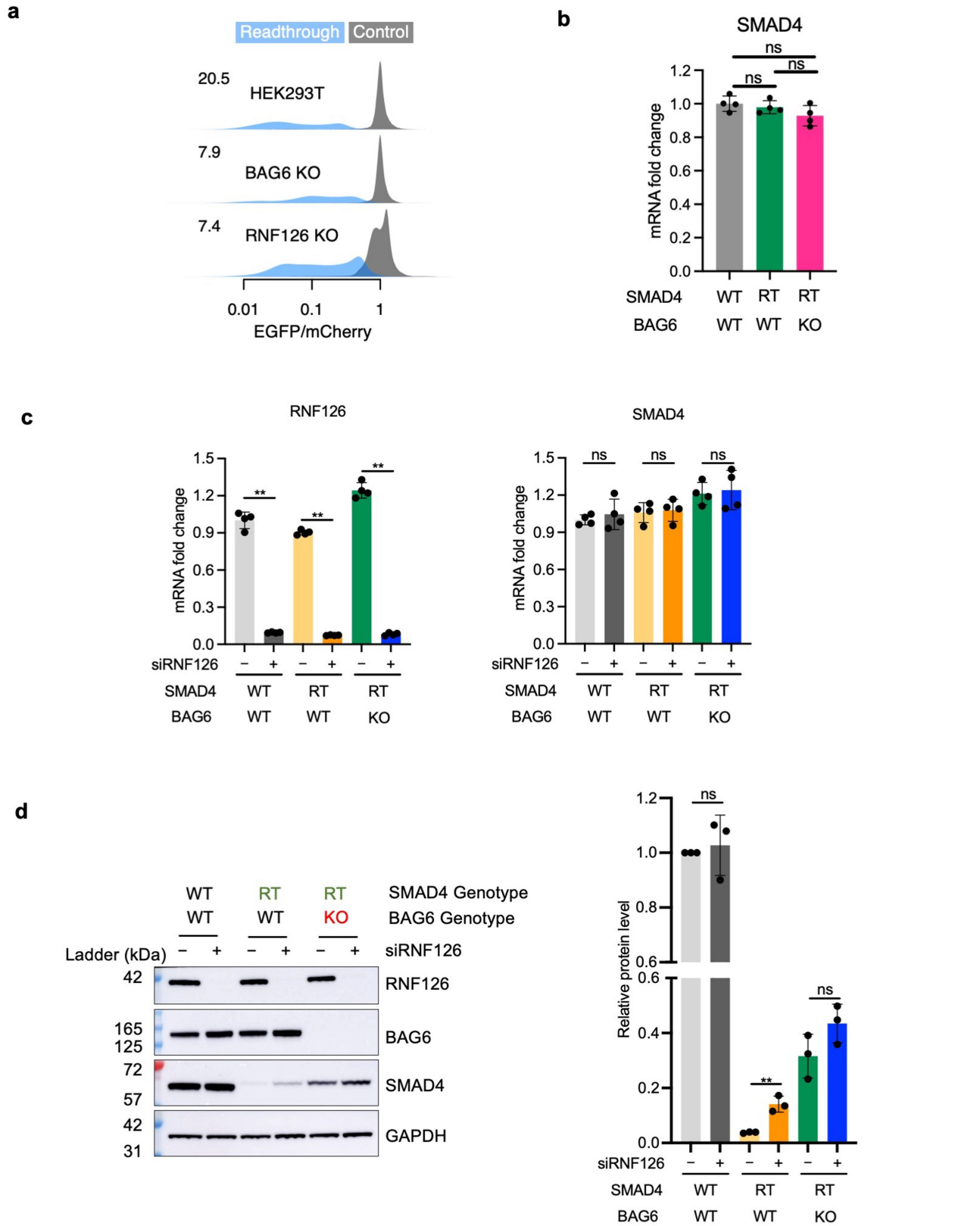

Extended Data Fig. 10 | BAG6 and RNF126 mediate the degradation of SMAD4 readthrough products. a, A dual color reporter fusing *SMAD4* 3′ UTR encoded peptide to the C-terminus of EGFP was tested in wild-type HEK293T cells, BAG6 KO cells, and RNF126 KO cells using flow cytometry as a readout. The number on the top left corner of each density plot is the median fold loss of EGFP/mCherry in the readthrough reporter relative to control. **b**, No significant change of SMAD4 mRNA level with BAG6 KO. RT: readthrough. N = 4 biologically independent samples. Data are presented as mean values +/− s.d. **c**, Efficient RNF126 knockdown and the lack of impact on endogenous SMAD4 mRNA (qRT-PCR). N = 4 biologically independent samples. Data are presented as mean values +/− s.d. **d**, Endogenous SMAD4 readthrough protein is stabilized by both BAG6 KO and RNF126 knockdown. Representative western blots on the left and quantification on the right. N = 3 biologically independent samples. Data are presented as mean values +/− s.d. One-way ANOVA was used for statistical analysis, with $P < 0.05$ considered significant. **: $P < 0.01$. No adjustments were made for multiple comparisons.

nature portfolio

Corresponding author(s): Xuebing Wu

Last updated by author(s): Mar 1, 2023

Reporting Summary

Nature Portfolio wishes to improve the reproducibility of the work that we publish. This form provides structure for consistency and transparency in reporting. For further information on Nature Portfolio policies, see our Editorial Policies and the Editorial Policy Checklist.

Statistics

For all statistical analyses, confirm that the following items are present in the figure legend, table legend, main text, or Methods section.

n/a	Confirmed
☐	☒ The exact sample size (*n*) for each experimental group/condition, given as a discrete number and unit of measurement
☐	☒ A statement on whether measurements were taken from distinct samples or whether the same sample was measured repeatedly
☐	☒ The statistical test(s) used AND whether they are one- or two-sided *Only common tests should be described solely by name; describe more complex techniques in the Methods section.*
☒	☐ A description of all covariates tested
☐	☒ A description of any assumptions or corrections, such as tests of normality and adjustment for multiple comparisons
☐	☒ A full description of the statistical parameters including central tendency (e.g. means) or other basic estimates (e.g. regression coefficient) AND variation (e.g. standard deviation) or associated estimates of uncertainty (e.g. confidence intervals)
☐	☒ For null hypothesis testing, the test statistic (e.g. *F*, *t*, *r*) with confidence intervals, effect sizes, degrees of freedom and *P* value noted *Give P values as exact values whenever suitable.*
☒	☐ For Bayesian analysis, information on the choice of priors and Markov chain Monte Carlo settings
☒	☐ For hierarchical and complex designs, identification of the appropriate level for tests and full reporting of outcomes
☐	☒ Estimates of effect sizes (e.g. Cohen's *d*, Pearson's *r*), indicating how they were calculated

Our web collection on statistics for biologists contains articles on many of the points above.

Software and code

Policy information about availability of computer code

Data collection	Adobe illustrator 2023 Illumina HiSeq 2000 Illumina NextSeq 550 Bio-Rad ZE5 NovoCyte Quanteon analyzer BD FACSAria II Fujifilm LAS3000 Amersham Imager 600 QuantStudio™ 7 Flex Real-Time PCR System
Data analysis	GraphPad Prisim 9 Microsoft Excel 16.70 FCS express 7 ImageJ 1.53 bedtools v2 bowtie version 1.2.3 MAGeCK v1 S4PRED v1 NCBI CDD: Conserved Domain Database, 2022 kpLogo v1, http://kplogo.wi.mit.edu/ ICE CRISPR Analysis Tool, v3, https://www.synthego.com/products/bioinformatics/crispr-analysis

Scripts (GNU bash 3.2.57, Python 3.7.4, and R 4.1.1) used for data analysis were deposited in GitHub: https://github.com/xuebingwu/noncoding-translation-code.

For manuscripts utilizing custom algorithms or software that are central to the research but not yet described in published literature, software must be made available to editors and reviewers. We strongly encourage code deposition in a community repository (e.g. GitHub). See the Nature Portfolio guidelines for submitting code & software for further information.

Data

Policy information about availability of data

All manuscripts must include a data availability statement. This statement should provide the following information, where applicable:

- Accession codes, unique identifiers, or web links for publicly available datasets
- A description of any restrictions on data availability
- For clinical datasets or third party data, please ensure that the statement adheres to our policy

The sequencing data for the massively parallel reporter assay has been deposited in GEO with the accession number GSE208661. Uncropped gel images were included in Supplementary Fig. 1. Gating strategies for flow cytometry assays were included in Supplementary Fig. 2.

Human research participants

Policy information about studies involving human research participants and Sex and Gender in Research.

Reporting on sex and gender	No human participants involved
Population characteristics	No human participants involved
Recruitment	No human participants involved
Ethics oversight	No human participants involved

Note that full information on the approval of the study protocol must also be provided in the manuscript.

Field-specific reporting

Please select the one below that is the best fit for your research. If you are not sure, read the appropriate sections before making your selection.

☒ Life sciences ☐ Behavioural & social sciences ☐ Ecological, evolutionary & environmental sciences

For a reference copy of the document with all sections, see nature.com/documents/nr-reporting-summary-flat.pdf

Life sciences study design

All studies must disclose on these points even when the disclosure is negative.

Sample size	There was sample-size calculation performed. Detailed sample sizes are presented in the figure legends and / or methods sections. Sample size were based on similar studies: PMID 27281202, and PMID 28525757. For flow cytometry, typically > 10^6 cells were used for generating density plots of EGFP/mCherry ratios. Our pilot analyses suggested that density plots can be robustly estimated with >10^4 cells. For massively parallel reporter analyses, a minimal of 10^6 cells were collected for each bin of EGFP/mCherry ratio, which represents ~100x coverage of the the Pep30 library. For qPCR and western blots, typically a minimum of three biological replicates were used.
Data exclusions	No data were excluded from the analyses
Replication	All experiments presented in the study have been successfully replicated. For qPCR and western blots, typically a minimum of three biological replicates were used. For high-throughput sequencing experiments, only one or two biological replicates were used, as in a single experiment, thousands of reads serve as replicates for each sequence. For the competitive growth assay, some replicates collected failed Sanger sequencing (noisy trace) and were not used. Remaining data points are consistent with each other suggesting successful replications. See similar studies: PMID 27281202, PMID 28525757
Randomization	Randomization was not required in our study, because cells were assigned into different groups according to genotypes. See similar studies: PMID 27281202, PMID 28525757
Blinding	Blinding was not relevant in this study, because there was no subjective analyses performed in this study, and blinding is impossible or unlikely to affect the results. See similar studies: PMID 27281202, PMID 28525757

Reporting for specific materials, systems and methods

We require information from authors about some types of materials, experimental systems and methods used in many studies. Here, indicate whether each material, system or method listed is relevant to your study. If you are not sure if a list item applies to your research, read the appropriate section before selecting a response.

Materials & experimental systems

n/a	Involved in the study
☐	☒ Antibodies
☐	☒ Eukaryotic cell lines
☒	☐ Palaeontology and archaeology
☒	☐ Animals and other organisms
☒	☐ Clinical data
☒	☐ Dual use research of concern

Methods

n/a	Involved in the study
☒	☐ ChIP-seq
☐	☒ Flow cytometry
☒	☐ MRI-based neuroimaging

Antibodies

Antibodies used

Anti-BAG6, monoclonal mouse, clone 1B8D3, Proteintech, Cat. No. 666611IG150UL, WB
Anti-Cofilin, rabbit monoclonal, clone D3F9, CST, Cat. No. 5175S, WB
Anti-GAPDH, rabbit polyclonal, Invitrogen, Cat. No. PA1-988, WB
Anti-GAPDH, mouse monoclonal, clone D4C6R, CST, Cat. No. 97166S, WB
Anti-GET4 (TRC35), rabbit polyclonal, Abclonal, Cat. No. A16190, WB
Anti-GFP, rabbit monoclonal, clone D5.1, CST, Cat. No. 2956S, WB
Anti-GFP, goat polyclonal, R&D Systems, Cat. No. AF4240, WB and IP
Anti-Lamin A/C, rabbit polyclonal, Proteintech, Cat. No. 10298-1-AP, WB
Anti-mCherry, rabbit polyclonal, Proteintech, Cat. No. NBP225157SS, WB
Anti-mCherry, rabbit monoclonal, clone E5D8F, CST, Cat. No. 43590, WB
Anti-RNF126, mouse monoclonal, clone C-1, Santa Cruz Biotechnology, Cat. No. sc-376005, WB
Anti-SGTA, rabbit polyclonal, CST, Cat. No. 3349S, WB
Anti-SMAD4, rabbit monoclonal, clone D3M6U, CST, Cat. No. 38454S, WB
Anti-UBL4A, mouse monoclonal, clone OTI2E2, Invitrogen, Cat. No. MA525418, WB
Anti-Vinculin, rabbit monoclonal, clone E1E9V, CST, Cat. No. 13901S, WB
Anti-β-Tubulin, mouse monoclonal, clone D3U1W, CST, Cat. No. 86298S, WB
Anti-K48 Linkage Polyubiquitination, rabbit polyclonal, CST, Cat. No. 4289S, Proteasome activity assay
Anti-SMAD4, mouse monoclonal, clone B-8, Santa Cruz Biotechnology, Cat. No. sc-7966, WB and IP

Validation

With the exception of BAG6/RNF126/UBL4A/SGTA/TRC35 antibodies validated with our human clonal KO HEK293T cells for western blotting, other antibodies were not empirically validated by us, but appropriate controls were used for each experiment to ensure the accurate findings. Additionally, validation information for each antibody can be found on the vendor's website.

Eukaryotic cell lines

Policy information about cell lines and Sex and Gender in Research

Cell line source(s)

HEK293T cells used in this study were purchased from ATCC. For experiments involving the SMAD4 gene, clonal cell lines harboring SMAD4 readthrough mutations as well as the parental HEK293T cells were obtained as a generous gift from Dr. Sven Diederichs.

Authentication

Not tested

Mycoplasma contamination

All cell lines, including both wild-type HEK293T, BAG6/RNF126/UBL4A/SGTA/TRC35 KO, and SMAD4 readthrough HEK293T cells used in this study were confirmed to be negative for Mycoplasma contamination and routinely tested negative using the MycoAlert mycoplasma detection kit (Lonza, LT07-418).

Commonly misidentified lines
(See ICLAC register)

None

Flow Cytometry

Plots

Confirm that:

☒ The axis labels state the marker and fluorochrome used (e.g. CD4-FITC).

☒ The axis scales are clearly visible. Include numbers along axes only for bottom left plot of group (a 'group' is an analysis of identical markers).

☒ All plots are contour plots with outliers or pseudocolor plots.

☒ A numerical value for number of cells or percentage (with statistics) is provided.

Methodology

Sample preparation	Cells were collected and resuspended in 1-4mL of fresh media and passed through a 35 um mesh cell strainer immediately prior to flow cytometry.
Instrument	Flow cytometry was performed on either a Bio-Rad ZE5 or NovoCyte Quanteon analyzer
Software	Gating of samples and export of data for downstream analysis was done using the FCS Express software
Cell population abundance	A minimum of 10^6 cells were analyzed for most experiments.
Gating strategy	Only live cell and singlet gating were used.

☒ Tick this box to confirm that a figure exemplifying the gating strategy is provided in the Supplementary Information.